Speed of sound and isothermal compressibility in a magnetized quark matter with anomalous magnetic moment of quarks

Rajkumar Mondal,[1,3,*] Sourav Duari,[1,†] Nilanjan Chaudhuri,[1,3,‡] Sourav Sarkar,[1,3,§] and Pradip Roy[2,3,‖]

[1]*Variable Energy Cyclotron Centre, 1/AF Bidhannagar, Kolkata 700064, India*
[2]*Saha Institute of Nuclear Physics, 1/AF Bidhannagar, Kolkata 700064, India*
[3]*Homi Bhabha National Institute, Training School Complex, Anushaktinagar, Mumbai 400085, India*

(Received 20 June 2024; accepted 12 August 2024; published 11 September 2024)

We study the characteristics of quark matter under the influence of a background magnetic field with an anomalous magnetic moment of quarks at finite temperature and quark chemical potential in the framework of a Polyakov loop extended Nambu-Jona-Lasinio model. In the presence of a magnetic field, the speed of sound and isothermal compressibility become anisotropic with respect to the direction of the background magnetic field, splitting into parallel and perpendicular directions with respect to the magnetic field. Though the qualitative nature of parallel and perpendicular components of squared speed of sound appear similar, they differ in magnitude at lower values of temperature. The parallel and perpendicular components of isothermal compressibility decrease with increasing temperature, indicating a trend towards increased incompressible strongly interacting matter. On inclusion of the anomalous magnetic moment of quarks, the perpendicular component of isothermal compressibility becomes greater than the parallel component. Additionally, we investigate the quark number susceptibility normalized by its value at zero magnetic field, which may indicate the presence of magnetic fields in the system.

DOI: 10.1103/PhysRevD.110.054010

I. INTRODUCTION

In recent times, the study of properties of matter under extreme conditions such as high temperature and/or density has been extended to include strong magnetic fields. Presently, it is well accepted that strong magnetic fields could exist in heavy ion collision (HIC) experiments at the Relativistic Heavy Ion Collider or Large Hadron Collider, in the cores of neutron stars, and during the early Universe. The estimated value of the magnetic field in the HIC experiment is around 10^{15-18} Gauss [1–3] generated by the rapid movement of electrically charged spectators in the early stages of the collision. Although it experiences rapid decay within a few fm/c, the finite electrical conductivity (∼a few MeV) of the medium can possibly delay the decay process sufficiently allowing a nonzero magnetic field to persist even during the subsequent hadronic phase following the phase transition or crossover from the quark-gluon plasma [4–6]. The magnitude of the magnetic field in astrophysical objects such as the interior of neutron stars, magnetars is of the order of 10^{15} Gauss. The strength of these magnetic fields is comparable to the typical energy scale of quantum chromodynamics (QCD), affecting various microscopic and macroscopic properties of strongly interacting matter (see Refs. [7–9] for reviews). Furthermore, the presence of background magnetic field results in a large number of interesting phenomena such as chiral magnetic effect [1,10–12], magnetic catalysis (MC) [13–16], inverse magnetic catalysis (IMC) etc. [17,18].

The spontaneous breakdown of chiral symmetry and color confinement are fundamental to the QCD vacuum at low energies. Due to the nonperturbative nature of QCD in this energy domain first principle calculations are untenable. Though lattice QCD (LQCD) simulations provide some useful insights at zero baryon density, the extension to finite chemical potentials is plagued with complications [19–22]. Consequently, phenomenological models are used to probe the thermodynamic and spectral properties of strongly interacting matter at low energies [23–25]. The Nambu-Jona-Lasinio (NJL) model [26,27] is one such extensively used model which respects the global symmetries of QCD, especially chiral symmetry. It is nonrenormalizable due to the pointlike quark interactions, which arises from integrating out the gluonic degrees of

*Contact author: rajkumarmondal.phy@gmail.com
†Contact author: s.duari@vecc.gov.in; sduari.vecc@gmail.com
‡Contact author: nilanjan.vecc@gmail.com; n.chaudhri@vecc.gov.in
§Contact author: sourav.vecc@gmail.com; sourav@vecc.gov.in
‖Contact author: pradipk.roy@saha.ac.in

freedom in this effective description [23,28]. Hence, a proper regularization scheme is needed to tame the divergent integrals. The model parameters are fixed by reproducing phenomenological quantities like the pion-decay constant, quark condensate, pion mass, and so on. However, the NJL model lacks confinement. To address both chiral symmetry breaking and quark confinement, the Polyakov loop extended NJL (PNJL) model introduces interactions between quarks and a static, homogeneous gluonlike field [29,30]. Significant study has been found in literature where PNJL model is used to investigate the deconfinement transition and chiral symmetry restoration in strongly interacting magnetized matter [9,31–37]. The presence of a uniform background magnetic field tends to catalyze the chiral condensate. This leads to an increase in the transition temperature from chiral symmetry broken to the restored phase with increasing magnetic field, known as MC [14,16]. As a result the transition temperature from chiral symmetry broken to the restored phase also increases. Results from LQCD simulations at higher temperatures however show an opposite trend indicating IMC of the transition temperature [38,39]. To address this discrepancy in NJL-type models extensive efforts have been put in [40–45]. An interesting alternative stems from the consideration of nonzero values of the anomalous magnetic moment (AMM) of the quarks which results in a decrease in chiral transition temperature implying IMC [32,46–55].

In a magnetized medium, the spatial component of the energy-momentum tensor in the presence of magnetic field becomes anisotropic due to the breaking of rotational symmetry [56–58]. This affects the equation of state (EOS) of strongly interacting matter. As a result, the pressure becomes direction dependent, varying with the orientation of the magnetic field. The anisotropy in pressure is studied in magnetized quark matter with AMM in Ref. [59]. In literature, numerous studies focus on investigating the EOS of compact stars such as neutron stars, quark stars, and hybrid stars, incorporating the anisotropic nature of pressure with substantial implications [56,60–70]. However, the current generating magnetic field is not considered and the system is assumed as boundaryless in the above studies.

The speed of sound reflects the propagation of disturbances through the medium. It is influenced by thermodynamic variables such as pressure, volume, temperature, and chemical potential, and, therefore, it is directly correlated with the EOS of the system. Hence, speed of sound can be used as an ideal probe for studying strongly interacting matter during its space-time evolution. It provides crucial insights, exhibiting a local minimum during a crossover and approaching zero at the critical point and along corresponding spinodal lines. Therefore, it is a suitable candidate for studying the phase structure of QCD. As discussed, the presence of a magnetic field induces anisotropy in pressure, which subsequently impacts the speed of sound, leading to different values depending on the direction of the magnetic field. Lattice QCD calculation demonstrates a minimum in the speed of sound at temperature $T_0 = 156.5 \pm 1.5$ MeV, indicating a crossover between hadron gas and quark-gluon plasma [71]. The speed of sound in QCD matter has been determined using various methods including LQCD [72–75], the (P)NJL model [76–79], the quark-meson coupling model [80,81], the hadron resonance gas model [82,83], the field correlator method [84,85], MIT bag model [86,87], and the quasiparticle model [88]. Additionally, the speed of sound holds particular significance for the studies of compact star properties. It has a substantial impact on the mass-radius relationship, cooling rate, the maximum possible mass of a neutron star [89], and tidal deformability. Analysis of current neutron star data indicate a substantial increase in the speed of sound at densities beyond the nuclear saturation density [90–93]. Furthermore, as indicated in Ref. [94], the speed of sound has crucial impact on the frequencies of gravitational waves generated by the g-mode oscillation of a neutron star.

Isothermal compressibility is an important parameter whose value indicates the relative stiffness of EOS. It is also relevant in the analysis of the phase structure of the system. In the presence of magnetic field, pressure anisotropy affects isothermal compressibility and takes different values depending on the direction of magnetic fields. Reference [95] investigates compressibility of rotating black holes. References [96–98] explore compressibility in quark matter, revealing insights into phase transitions and magnetic field effects.

The quark number susceptibility measures the response of the number density to an infinitesimal change of the quark chemical potential and is closely related to the fluctuations of conserved quantities, such as baryon number and electric charge. In recent times, there has been notable interest in investigating fluctuations of conserved charges within a magnetic field background [99–102]. It is observed that a finite magnetic field significantly affects these observables, which are of direct phenomenological interest and can be measured experimentally.

Recently, we have studied characteristics of nuclear matter in presence of a background magnetic field in Ref. [103]. In the present article, we will study the speed of sound and isothermal compressibility in magnetized quark matter using the PNJL model, illustrating the dependency of these observables on the AMM of quarks. Additionally, we investigate the quark number susceptibility, normalized by its zero field value, which may be an indicator for the existence of magnetic field in the system.

The article is organized as follows: Sec. II gives a brief introduction to the general formalism of the PNJL model, while Sec. III elaborates on the expressions for speed of

sound in different thermodynamic situations and the isothermal compressibility. Section IV discusses results, with a summary and conclusion provided in Sec. V. Further details are given in the Appendix.

II. PNJL MODEL

The PNJL model is an effective model of strongly interacting matter that combines chiral symmetry breaking with the effects of Polyakov loop which represents the deconfinement aspects of the matter. The Lagrangian density of the two-flavor PNJL model taking into account the AMM of free quarks in the presence of a constant background magnetic field can be expressed as follows [32,46,47,59]:

$$\mathcal{L} = \bar{q}(x)\left(i\gamma^{\mu}D_{\mu} - m + \gamma^{0}\mu_{q} + \frac{1}{2}\hat{a}\sigma^{\mu\nu}F_{\mu\nu}\right)q(x) + G\{(\bar{q}(x)q(x))^{2} + (\bar{q}(x)i\gamma_{5}\tau q(x))^{2}\} - U(\Phi,\bar{\Phi},T). \tag{1}$$

Here, $q(x)$ represents the quark doublet fields where we have omitted the flavor ($f = u, d$) and color ($c = r, g, b$) indices from the quark field ($q^{fc}(x)$) for convenience, m is the current quark mass with $m_u = m_d = m$ to ensure the isospin symmetry of the theory at vanishing magnetic field, μ_q represents quark chemical potential, $F_{\mu\nu} = (\partial_\mu A_\nu - \partial_\nu A_\mu)$ is the electromagnetic field strength tensor, and $\sigma^{\mu\nu} = \frac{i}{2}\{\gamma^\mu\gamma^\nu - \gamma^\nu\gamma^\mu\}$. The constituent quarks interact with the Abelian gauge field A_μ and $\mathrm{SU_c}(3)$ gauge field A^a_μ via the covariant derivative:

$$D_\mu = \partial_\mu - i\hat{Q}A_\mu - iA^a_\mu, \tag{2}$$

where A_μ describes the vector potential of the external magnetic field along $\hat{z}$ direction [for Landau gauge $A_\mu = (0, 0, xB, 0)$], the electric charge of quark is $\hat{Q} = \mathrm{diag}(2e/3, -e/3)$, $\hat{a} = \hat{Q}\hat{\kappa}$, where $\hat{\kappa} = \mathrm{diag}(\kappa_u, \kappa_d)$ is a matrix in flavor space containing AMM of the quarks. In this work we adopt the logarithmic form which is given by [104]

$$U(\Phi,\bar{\Phi},T) = T^4\left[-\frac{1}{2}A(T)\bar{\Phi}\Phi + B(T)\ln\{1 - 6\bar{\Phi}\Phi + 4(\bar{\Phi}^3 + \Phi^3) - 3(\bar{\Phi}\Phi)^2\}\right] \tag{3}$$

$$\text{with}\quad A(T) = a_0 + a_1\left(\frac{T_0}{T}\right) + a_2\left(\frac{T_0}{T}\right)^2, \qquad B(T) = b_3\left(\frac{T_0}{T}\right)^3. \tag{4}$$

Here the logarithmic divergence of the Polyakov loop potential as $\Phi, \bar{\Phi} \to 1$ in the Haar measure formulation ensures that the Polyakov loop Φ remains physically bounded and approaches its maximum value of 1 only at asymptotically high temperatures. However, as shown in Ref. [32], the results are qualitatively similar for different choices of Polyakov loop potential. The parameters of the model are provided in Table I [59,104,105]. Now, employing a mean field approximation on the Lagrangian provided in Eq. (1), one can obtain the thermodynamic potential for two-flavor PNJL model using imaginary time formalism of finite temperature field theory as [32,59,106]

$$\Omega = \frac{B^2}{2} + \frac{(M - m_0)^2}{4G} + U(\Phi,\bar{\Phi},T) - 3\sum_{nfs}\frac{|e_fB|}{2\pi}\int_{-\infty}^{+\infty}\frac{dp_z}{2\pi}\omega_{nfs}f_\Lambda - T\sum_{nfs}\frac{|e_fB|}{2\pi}\int_{-\infty}^{+\infty}\frac{dp_z}{2\pi}\{\ln g^+ + \ln g^-\}, \tag{5}$$

where n is the Landau level, $s \in (\pm 1)$, and

$$g^+ = g^+(\Phi,\bar{\Phi},T,\mu_q) = 1 + 3(\Phi + \bar{\Phi}e^{-\frac{\omega_{nfs}-\mu_q}{T}})e^{-\frac{\omega_{nfs}-\mu_q}{T}} + e^{-3\frac{\omega_{nfs}-\mu_q}{T}}, \tag{6}$$

$$g^- = g^-(\Phi,\bar{\Phi},T,\mu_q) = g^+(\bar{\Phi},\Phi,T,-\mu_q). \tag{7}$$

TABLE I. Parameters in PNJL model [59,104,105].

T_0 (GeV)	a_0	a_1	a_2	a_3	G
0.270	3.51	−2.47	15.2	−1.7	$2.2/\Lambda^2$

The PNJL model is known to be nonrenormalizable due to the pointlike interactions between the quarks [23]. Consequently, a regularization scheme is to be chosen to eliminate divergences in the medium-independent term in Eq. (5). In a magnetic field, the sharp momentum cutoff causes artifacts due to the replacement of continuous momentum with discrete Landau levels. Here, we have opted for the smooth cutoff regularization procedure and introduced a multiplicative form factor [59,105], which is given by the expression

$$f_\Lambda = \frac{\Lambda^{2N}}{\Lambda^{2N} + \{p_z^2 + (2n + 1 - s)|e_fB|\}^N} \tag{8}$$

in Eq. (5) to tame the divergent medium-independent integral. The parameters N and Λ are chosen to reproduce the vacuum values of the pion decay constant f_π and the pion mass m_π. The energy eigenvalues of the quarks in the presence of a background magnetic field with AMM of quarks is obtained as

$$\omega_{nfs} = \sqrt{p_z^2 + \left\{\sqrt{M^2 + (2n+1-s)|e_f B|} - s\kappa_f e_f B\right\}^2}. \quad (9)$$

The constituent quark mass M and the expectation values of the Polyakov loops Φ and $\bar{\Phi}$ can be obtained self-consistently from Eq. (1) by using the stationary conditions

$$\frac{\partial\Omega}{\partial M} = 0, \qquad \frac{\partial\Omega}{\partial\Phi} = 0, \qquad \frac{\partial\Omega}{\partial\bar{\Phi}} = 0. \quad (10)$$

Now, using Eqs. (5) and (10) leads to the following coupled equations [32,59]:

$$M = m + 6G\sum_{nfs}\frac{|e_f B|}{2\pi}\int_{-\infty}^{+\infty}\frac{dp_z}{2\pi}\frac{1}{\omega_{nfs}} \times \frac{M}{M_{nfs}}\{M_{nfs} - s\kappa_f e_f B\}(1 - f^+ - f^-), \quad (11)$$

$$\frac{\partial U}{\partial\Phi} = 3T\sum_{nfs}\frac{|e_f B|}{2\pi}\int_{-\infty}^{+\infty}\frac{dp_z}{2\pi}\left\{\frac{e^{-\frac{\omega_{nfs}-\mu_q}{T}}}{g^+} + \frac{e^{-2\frac{\omega_{nfs}+\mu_q}{T}}}{g^-}\right\}, \quad (12)$$

$$\frac{\partial U}{\partial\bar{\Phi}} = 3T\sum_{nfs}\frac{|e_f B|}{2\pi}\int_{-\infty}^{+\infty}\frac{dp_z}{2\pi}\left\{\frac{e^{-2\frac{\omega_{nfs}-\mu_q}{T}}}{g^+} + \frac{e^{-\frac{\omega_{nfs}+\mu_q}{T}}}{g^-}\right\}, \quad (13)$$

where

$$M_{nfs} = \sqrt{M^2 + (2n+1-s)|e_f B|}, \quad (14)$$

$$f^+ = f^+(\Phi, \bar{\Phi}, T, \mu_q) = \frac{1}{g^+}\left\{\left(\Phi + 2\bar{\Phi}e^{-\frac{\omega_{nfs}-\mu_q}{T}}\right)e^{-\frac{\omega_{nfs}-\mu_q}{T}} + e^{-3\frac{\omega_{nfs}-\mu_q}{T}}\right\}, \quad (15)$$

$$f^- = f^-(\Phi, \bar{\Phi}, T, \mu_q) = f^+(\bar{\Phi}, \Phi, T, -\mu_q). \quad (16)$$

$\frac{\partial U}{\partial\Phi}$ and $\frac{\partial U}{\partial\bar{\Phi}}$ are obtained from Eq. (3) and expressed as

$$\frac{\partial U}{\partial\Phi} = \frac{\partial U(\Phi, \bar{\Phi}, T)}{\partial\Phi} = -T^4\left\{\frac{1}{2}A(T)\bar{\Phi} + 6B(T)\frac{\bar{\Phi} - 2\Phi^2 + (\bar{\Phi}\Phi)\bar{\Phi}}{1 - 6\bar{\Phi}\Phi + 4(\Phi^3 + \overline{\Phi^3}) - 3(\bar{\Phi}\Phi)^2}\right\}, \quad (17)$$

$$\frac{\partial U}{\partial\bar{\Phi}} = \frac{\partial U(\Phi, \bar{\Phi}, T)}{\partial\Phi}(\Phi \to \bar{\Phi}, \bar{\Phi} \to \Phi). \quad (18)$$

Furthermore, the expressions for quark the number density, entropy density, and magnetization are obtained as follows [32,59]:

$$n_q = -\frac{\partial\Omega}{\partial\mu_q} = 3\sum_{nfs}\frac{|e_f B|}{2\pi}\int_{-\infty}^{+\infty}\frac{dp_z}{2\pi}\{f^+ - f^-\}, \quad (19)$$

$$s = -\frac{\partial\Omega}{\partial T} = -\frac{\partial U}{\partial T} + \sum_{nfs}\frac{|e_f B|}{2\pi}\int_{-\infty}^{+\infty}\frac{dp_z}{2\pi}\{\ln g^+ + \ln g^-\} + 3T\sum_{nfs}\frac{|e_f B|}{2\pi}\int_{-\infty}^{+\infty}\frac{dp_z}{2\pi}\left\{\frac{\omega_{nfs}-\mu_q}{T^2}f^+ + \frac{\omega_{nfs}+\mu_q}{T^2}f^-\right\}, \quad (20)$$

$$\mathcal{M} = -\frac{\partial\Omega}{\partial B} = -B + 3\sum_{nfs}\frac{|e_f|}{2\pi}\int_{-\infty}^{+\infty}\frac{dp_z}{2\pi}\omega_{nfs}f_\Lambda + 3\sum_{nfs}\frac{|e_f B|}{2\pi}\int_{-\infty}^{+\infty}\frac{dp_z}{2\pi}\omega_{nfs}\frac{\partial f_\Lambda}{\partial B} + T\sum_{nfs}\frac{|e_f|}{2\pi}\int_{-\infty}^{+\infty}\frac{dp_z}{2\pi}\{\ln g^+ + \ln g^-\} + 3\sum_{nfs}\frac{|e_f B|}{2\pi}\int_{-\infty}^{+\infty}\frac{dp_z}{2\pi}\frac{1}{\omega_{nfs}}\left\{1 - \frac{s\kappa_f e_f B}{M_{nfs}}\right\}\left\{\frac{2n+1-s}{2}|e_f| - s\kappa_f e_f M_{nfs}\right\}\{f_\Lambda - f^+ - f^-\}, \quad (21)$$

where the expression for $\frac{\partial f_\Lambda}{\partial B}$ can be found in Appendix A. Note that the expressions for all the thermodynamic quantities in absence of AMM can be obtained by putting $\kappa = 0$, which agree with those in Refs. [9,107]. To arrive at the results for $eB = 0$; i.e., for a thermal medium one has to make the replacement

$$\sum_{nfs}\frac{|e_f B|}{2\pi}\int_{-\infty}^{+\infty}\frac{dp_z}{2\pi} \to \int\frac{d^3p}{(2\pi)^3} \quad \text{and} \quad \omega_{nfs} \to \omega_p = \sqrt{\vec{p}^2 + M^2}, \quad (22)$$

compare with Ref. [108].

III. SPEED OF SOUND AND ISOTHERMAL COMPRESSIBILITY

The speed of sound is calculated as the square root of the ratio between a change in pressure (p) and the corresponding shift in energy density (ϵ). Typically, the determination of sound speed generally involves specifying a constant parameter, denoted as x, where $x \equiv s/n_q$, s, n_q, T, μ_q etc. during the propagation of a compression wave through a medium. It is defined as

$$c_x^2 = \left(\frac{\partial p}{\partial \epsilon}\right)_x. \tag{23}$$

When the speed of sound is used to study the hydrodynamic evolution of the hot and dense matter created in heavy ion collisions, it is essential to consider the appropriate trajectory through the QCD phase diagram. This is usually achieved by following isentropic curves such that the entropy per baryon (or entropy density per baryon density) s/n_q is constant [109]. Additionally, it is also interesting to calculate the squared speed of sound with constant T and μ_q. For example, c_T^2 is commonly used when there is a temperature reservoir or when the cooling timescale is fast compared to the sound wave period. Such a physical scenario may exist in the interstellar medium [110]. In this article, we will study the sound speed in quark matter in a background magnetic field. The expressions for longitudinal and transverse components of the pressure and energy density are as follows [56,58]:

$$\epsilon = \Omega + Ts + \mu_q n_q, \tag{24}$$

$$p^{\parallel} = -\Omega, \qquad p^{\perp} = p^{\parallel} - B\mathcal{M}. \tag{25}$$

Correspondingly, the speed of sound becomes anisotropic due to the presence of a magnetic field. We will define the speed of sound using various thermodynamic relations expressed in terms of temperature T and μ_q as [103]

$$c_x^2(T,\mu_q) = c_x^{2(\parallel)}(T,\mu_q) = \left(\frac{\partial p^{\parallel}}{\partial \epsilon}\right)_x = \frac{\partial(p^{\parallel},x)}{\partial(\epsilon,x)} = \frac{\partial(p^{\parallel},x)/\partial(T,\mu_q)}{\partial(\epsilon,x)/\partial(T,\mu_q)} = \frac{\left(\frac{\partial p^{\parallel}}{\partial T}\right)_{\mu_q}\left(\frac{\partial x}{\partial \mu_q}\right)_T - \left(\frac{\partial p^{\parallel}}{\partial \mu_q}\right)_T\left(\frac{\partial x}{\partial T}\right)_{\mu_q}}{\left(\frac{\partial \epsilon}{\partial T}\right)_{\mu_q}\left(\frac{\partial x}{\partial \mu_q}\right)_T - \left(\frac{\partial \epsilon}{\partial \mu_q}\right)_T\left(\frac{\partial x}{\partial T}\right)_{\mu_q}}, \tag{26}$$

$$c_x^{2(\perp)}(T,\mu_q) = \left(\frac{\partial p^{\perp}}{\partial \epsilon}\right)_x = c_x^{2(\parallel)} - B\left(\frac{\partial \mathcal{M}}{\partial \epsilon}\right)_x = c_x^{2(\parallel)} - B\frac{\left(\frac{\partial \mathcal{M}}{\partial T}\right)_{\mu_q}\left(\frac{\partial x}{\partial \mu_q}\right)_T - \left(\frac{\partial \mathcal{M}}{\partial \mu_q}\right)_T\left(\frac{\partial x}{\partial T}\right)_{\mu_q}}{\left(\frac{\partial \epsilon}{\partial T}\right)_{\mu_q}\left(\frac{\partial x}{\partial \mu_q}\right)_T - \left(\frac{\partial \epsilon}{\partial \mu_q}\right)_T\left(\frac{\partial x}{\partial T}\right)_{\mu_q}}, \tag{27}$$

where $c_x{}^{(\parallel)}$ and $c_x{}^{(\perp)}$ are the sound velocities along and perpendicular to the magnetic field direction, respectively. Using the thermodynamic relations given in Appendix B, we can further write down the sound velocity along the magnetic field direction as

$$c_{s/n_q}^{2(\parallel)} = \frac{n_q s\left(\frac{\partial s}{\partial \mu_q}\right)_T - s^2\left(\frac{\partial n_q}{\partial \mu_q}\right)_T - n_q^2\left(\frac{\partial s}{\partial T}\right)_{\mu_q} + s n_q\left(\frac{\partial n_q}{\partial T}\right)_{\mu_q}}{\left(sT+\mu_q n_q\right)\left\{\left(\frac{\partial s}{\partial \mu_q}\right)_T\left(\frac{\partial n_q}{\partial T}\right)_{\mu_q} - \left(\frac{\partial s}{\partial T}\right)_{\mu_q}\left(\frac{\partial n_q}{\partial \mu_q}\right)_T\right\}}, \tag{28}$$

and sound velocity perpendicular to the magnetic field direction as

$$c_{s/n_q}^{2(\perp)} = c_{s/n_q}^{2(\parallel)} - B\frac{n_q\left\{\left(\frac{\partial \mathcal{M}}{\partial T}\right)_{\mu_q}\left(\frac{\partial s}{\partial \mu_q}\right)_T - \left(\frac{\partial \mathcal{M}}{\partial \mu_q}\right)_T\left(\frac{\partial s}{\partial T}\right)_{\mu_q}\right\} - s\left\{\left(\frac{\partial \mathcal{M}}{\partial T}\right)_{\mu_q}\left(\frac{\partial n_q}{\partial \mu_q}\right)_T - \left(\frac{\partial \mathcal{M}}{\partial \mu_q}\right)_T\left(\frac{\partial n_q}{\partial T}\right)_{\mu_q}\right\}}{(sT+\mu_q n_q)\left\{\left(\frac{\partial s}{\partial \mu_q}\right)_T\left(\frac{\partial n_q}{\partial T}\right)_{\mu_q} - \left(\frac{\partial s}{\partial T}\right)_{\mu_q}\left(\frac{\partial n_q}{\partial \mu_q}\right)_T\right\}}. \tag{29}$$

The expressions for $\left(\frac{\partial \mathcal{M}}{\partial T}\right)_{\mu_q}$, $\left(\frac{\partial \mathcal{M}}{\partial \mu_q}\right)_T$, $\left(\frac{\partial s}{\partial \mu_q}\right)_T$, $\left(\frac{\partial s}{\partial T}\right)_{\mu_q}$, $\left(\frac{\partial n_q}{\partial \mu_q}\right)_T$, and $\left(\frac{\partial n_q}{\partial T}\right)_{\mu_q}$ in Eqs. (28) and (29) are provided in Appendix C.

In thermodynamics, isothermal compressibility is a measure of change in volume of the system with increasing pressure. It is considered a sensitive quantity for indicating the fluctuation of the order parameter during a phase transition. Its smaller value reflects relatively stiffer EOS. Mathematically, it is defined in the absence of a magnetic field as

$$K_T = -\frac{1}{V}\left(\frac{\partial V}{\partial P}\right)_T = \frac{1}{n_q^2}\left(\frac{\partial n_q}{\partial \mu_q}\right)_T. \tag{30}$$

Because of the anisotropy in pressure, the isothermal compressibility K_T splits into parallel and perpendicular components with respect to the direction of the magnetic field. The expressions for $K_T^{\parallel}$ and $K_T^{\perp}$ are given by

$$K_T^{(\parallel)} = \frac{1}{n_q^2}\left(\frac{\partial n_q}{\partial \mu_q}\right)_T, \tag{31}$$

$$K_T^{(\perp)} = \frac{1}{n_q\left\{n_q - B\left(\frac{\partial \mathcal{M}}{\partial \mu_q}\right)_T\right\}}\left(\frac{\partial n_q}{\partial \mu_q}\right)_T. \tag{32}$$

IV. NUMERICAL RESULTS

In this section, we present results for thermodynamic quantities in magnetized quark matter using the PNJL model under various physical situations. The model parameters are determined by fitting the empirical values of the pion decay constant $f_\pi = 92.4$ MeV and the pion mass $m_\pi = 138$ MeV and chiral condensate $(\langle \bar{u}u \rangle)^{1/3} = -245.7$ MeV at zero temperature and zero baryon density in the absence of a background magnetic field. Specifically, the model parameters are $\Lambda = 620$ MeV, $m = 5.5$ MeV. Since we are interested for the thermodynamic properties of magnetized quark matter, the choice of the representative values of background magnetic field $eB = 0.05$ GeV^2 and $eB = 0.10$ GeV^2 along with $eB = 0$ which will provide us the opportunity to explore the interplay between the magnetic field and the thermal effects. The AMM of quarks are taken as $\kappa_u = 0.29016$ GeV^{-1} and $\kappa_d = 0.35986$ GeV^{-1} [46,59]. In this section, we evaluate the results with a finite magnetic field, considering up to 2000 Landau levels for convergence.

A. Constituent quark mass

We start this section with the investigation of the constituent quark mass as a function of temperature, chemical potential and background magnetic field. This is achieved from the self-consistent solutions of Eqs. (11)–(13). Figure 1(a) shows the variation of constituent quark mass with temperature for several values of $\mu_q = 0.0, 0.1, 0.2$ MeV in the absence of magnetic field. The constituent quark mass starts at a high value and remains relatively stable at low temperatures indicating chirally broken phase. It then undergoes a rapid decrease within a narrow temperature range and eventually becomes nearly equal to the bare mass of quarks representing partial restoration of chiral symmetry. This transition occurs at $T^{\rm ch} \sim 230$ MeV in the absence of the magnetic field and zero chemical potential. As μ_q increases, Fig. 1(a) also depicts a decrease in the magnitude of M and a shift of the transition temperature towards lower values. In Figs. 1(b) and 1(c), the variation of constituent quark mass with temperature is shown for several values of μ_q at magnetic field strength $eB = 0.05$ and 0.10 GeV^2, respectively, considering both zero and nonzero values of AMM of quarks. It is observed that the constituent quark mass is greater in the scenario when quarks have zero AMM compared to when they have finite AMM [e.g., the cyan and red lines in the inset plot of Fig. 1(b)]. This difference becomes more evident with increasing magnetic field strength near the chiral phase transition [cyan and red lines in Figs. 1(b) and 1(c)].

Next, we will investigate the magnetic field dependence of constituent quark mass for various values of μ_q both with and without the AMM of quarks at three different temperatures representing various stages of the chiral phase. Analyzing Figs. 1(a)–1(c), the different stages are as follows:

(i) $T < T^{\rm ch}$ indicates the broken chirally symmetry phase. We select $T = 150$ MeV as a representative temperature to investigate this phase.
(ii) $T \sim T^{\rm ch}$ represents region near chiral phase transition. We take $T = 230$ MeV as a representative temperature to investigate this phase.
(iii) $T > T^{\rm ch}$ signifies partial restoration of chiral symmetry phase. We choose $T = 275$ MeV as a representative temperature to investigate this phase.

Figures 2(a)–2(c) illustrate the constituent quark mass as a function of background magnetic field for various values of

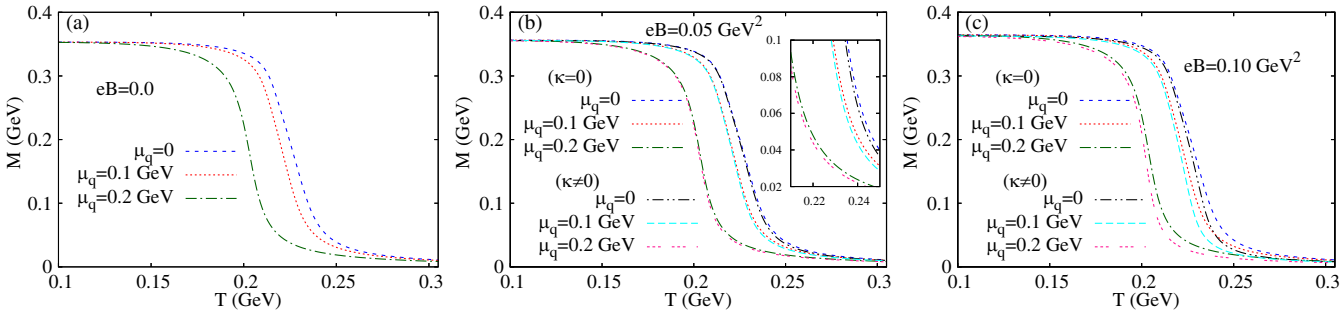

FIG. 1. Constituent quark mass (M) as function of temperature (T) for different values of chemical potentials $\mu_q = 0.0, 0.1, 0.2$ GeV at (a) $eB = 0$, (b) $eB = 0.05$ GeV^2, (c) $eB = 0.10$ GeV^2.

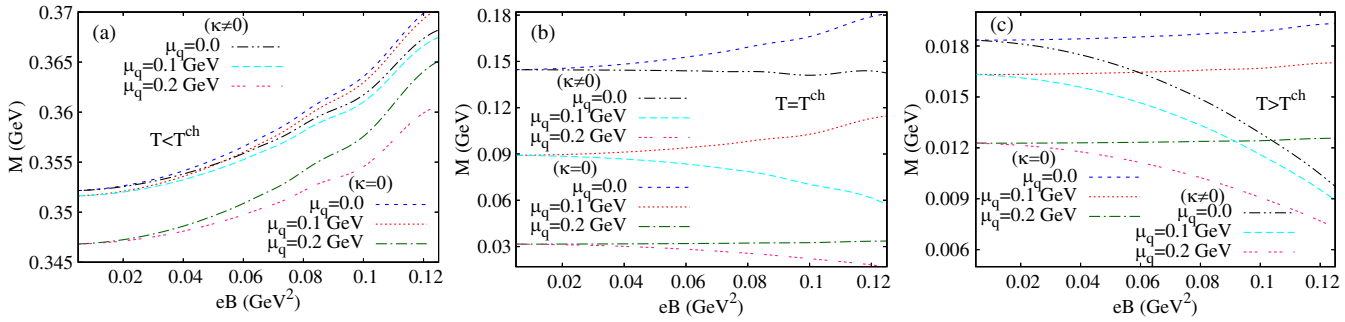

FIG. 2. Constituent quark mass (M) as function of background magnetic field (eB) for different values of chemical potentials $\mu_q = 0.0, 0.1, 0.2$ GeV at (a) $T = 150$ MeV, (b) $T = 230$ MeV, (c) $T = 275$ MeV.

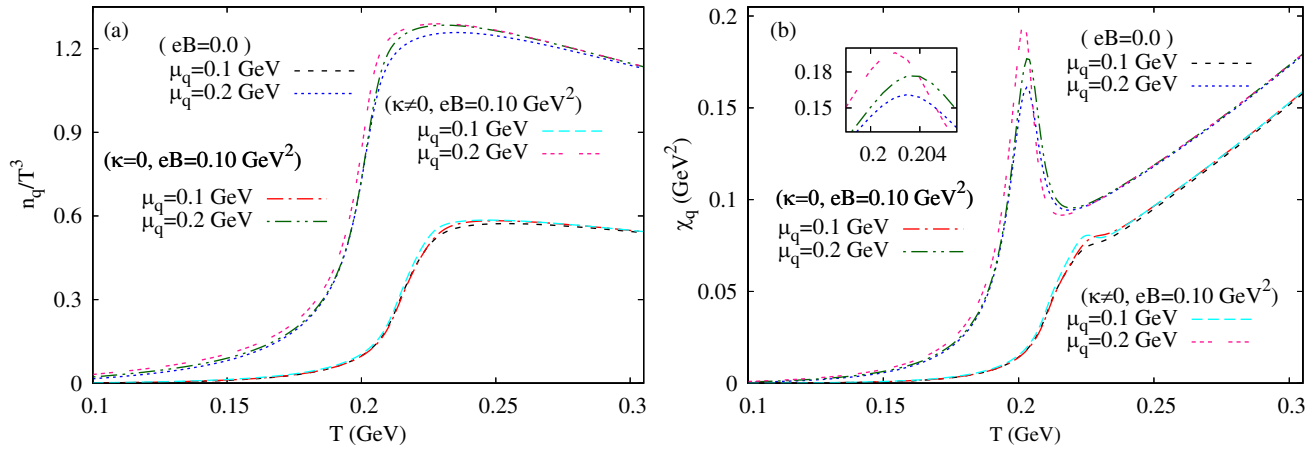

FIG. 3. Variation of (a) scaled quark number density (n_q/T^3) and (b) $\chi_q = \frac{dn_q}{d\mu_q}$ as function temperature (T) for different values of μ_q and eB.

μ_q at three different temperatures representing the different phases as mentioned before considering both scenarios with and without the AMM of quarks. In chirally broken phase as shown in Fig. 2(a), M increases with increasing eB for all mentioned values of μ_q irrespective of whether the AMM of quarks are included or not, which is known as the MC. However, the increase in M is slightly smaller with increasing eB at each values of μ_q when the AMM of quarks is included [e.g., blue and black lines in Figs. 2(a)]. Notably, the magnitude of M consistently appears higher for a smaller value of μ_q across all values of eB both with and without AMM of quarks. Near chiral phase transition as shown in Fig. 2(b), M increases with increasing eB in the absence of AMM of quarks. Conversely, an opposite trend is observed when AMM of quarks is present and this is known as IMC. As the temperature increases partial chiral symmetry has been restored as shown in Fig. 2(c). Here, the qualitative behavior of the plots are similar as observed in Fig. 2(b). Finally, in all the stages of phase transition the constituent quark mass difference between the zero and nonzero AMM of quarks increases with increase eB [e.g., black and blue lines in any of the subplots in Figs. 2(a)–2(c)], which is also evident from Figs. 1(a)–1(c).

B. Quark number density and quark number susceptibility

The scaled quark number density is defined as n_q/T^3. The behavior of the quark number density is investigated following Refs. [29,32]. The results for n_q/T^3 as a function of temperature are presented in Fig. 3(a) at $\mu_q = 0.1$ and 0.2 GeV considering the three cases: (i) $eB = 0.0$, (ii) $eB = 0.10$ GeV^2, $\kappa = 0$, (iii) $eB = 0.10$ GeV^2, $\kappa \neq 0$. For case (i), the interactions of an effective gluon field suppress contributions from both one-quark and two-quark states to the density below the transition temperature. As a result, the three-quark state becomes more dominant. Thus, we observe a strong suppression in the density of quarks below the transition. However, this suppression becomes less effective for temperatures above the transition [e.g., blue line in Fig. 3(a)]. This can be understood from Eqs. (15), (16), and (19) (see Ref. [59] for details). Moreover, it is evident that the scaled quark density rises as μ_q increases. The same qualitative behavior is also observed in the presence of background magnetic fields in case of (ii). This similarity arises because the change in M is almost negligible compared to the zero field case at high

temperature and the contributions from one-quark and two-quark states remain strongly suppressed in the low temperature region below the transition as in the zero field case. Furthermore, when we include the AMM of quarks, i.e., in case of (iii), the value of n_q/T^3 increases [see, e.g., magenta, blue, and green lines Fig. 3(a)] compared to cases of (i) and (ii).

Next, we focus on susceptibilities. For example, the chiral susceptibility carries signals of phase transitions and can be considered an order parameter for chiral transitions. The expression for the quark number susceptibility is given in Eq. (C6). Figure 3(b) shows the result for quark number susceptibilities (χ_q) varying with temperature for $\mu = 0.1$ and 0.2 GeV in the following three cases: (i) $eB = 0.0$, (ii) $eB = 0.10$ GeV^2, $\kappa = 0$, (iii) $eB = 0.10$ GeV^2, $\kappa \neq 0$. In the presence of background magnetic field, the transition temperature ($T_c^{\chi_q}$) shifts towards higher values [blue and green lines in the inset plot of Fig. 3(b)] indicating a MC. On the other hand, $T_c^{\chi_q}$ moves towards lower values of temperature when the AMM of quarks are included implying IMC [blue and magenta lines in the inset plot of Fig. 3(b)]. This can be observed from the inset plot in Fig. 3(b) at $\mu_q = 0.2$ GeV. As the quark chemical potential decreases, the discontinuity in the curves vanishes indicating a crossover [black, red, and cyan lines in Fig. 3(b)]. We now study the normalized susceptibility at three different temperatures where it is defined as the ratio of susceptibilities obtained in noncentral collisions (strong magnetic fields) to that of central collisions (weak or vanishing magnetic fields) following Refs. [99,100]. It is defined as

$$R_{\chi_q} = \frac{\chi_q(eB \neq 0)}{\chi_q(eB = 0)}. \tag{33}$$

Therefore, by definition, R_{χ_q} will be unity in central collisions or vanishing (weak) magnetic fields. So, R_{χ_q} can possibly be considered as a quantity sensitive to the existence of magnetic field in the system. Here, we will present R_{χ_q} as a function of eB for various values of μ_q with and without AMM of quarks at different stages of chiral phase transition as mentioned previously in Sec. IV A. Figures 4(a)–4(c) represent the stages as $T < T^{\rm ch}$, $T = T^{\rm ch}$, and $T > T^{\rm ch}$, respectively. In a chirally broken phase, Fig. 4(a) shows that R_{χ_q} has a rising nature with increasing magnetic fields and R_{χ_q} also increases with higher values of μ_q [see, e.g., red and green lines in Fig. 4(a)]. Furthermore, the overall magnitude of R_{χ_q} is larger with AMM of quarks [black and blue lines in Fig. 4(a)] but the behavioral nature is the same. In the vicinity of chiral phase transition Fig. 4(b) also shows that R_{χ_q} increases in presence of AMM of quarks. Figure 4(c) represents the partial chirally restored phase. Here R_{χ_q} exhibits a rising nature with increasing eB and its magnitude further increases with the inclusion of the AMM of quarks. However, R_{χ_q} decreases with higher values of μ_q with or without AMM of quarks. It is also evident from the Figs. 4(a)–4(c) that R_{χ_q} decreases with increasing temperature. Therefore, it can be concluded that the magnetic field effect is small in the partial chirally restored phase compared to the chirally broken and nearly restored phase.

C. Magnetization of the medium

The expression for the magnetization is given in Eq. (21). We define, for convenience, the scaled magnetization ($\mathcal{M}_{\rm Scaled}$) as

$$e\mathcal{M}_{\rm Scaled} = \mathcal{M}(T,\mu_q,eB) - \mathcal{M}(T=0,\mu_q=0,eB). \tag{34}$$

In Figs. 5(a)–5(c), we illustrate the variation of scaled magnetization ($\mathcal{M}_{\rm scaled}$) as a function of the background magnetic field for various values of μ_q both with and without the AMM of the quarks at three different temperatures representing chiral symmetry breaking, near chiral phase transition and its restoration respectively as discussed in Sec. IV A. In chirally broken phase, it is evident from Fig. 5(a) that $\mathcal{M}_{\rm Scaled}$ shows an oscillating trend as the magnetic field eB increases. The oscillating trend and magnitude of $\mathcal{M}_{\rm Scaled}$ increase as the temperature increases as evident in Figs. 5(a)–5(c). Finally, it is observed from each subplot that $\mathcal{M}_{\rm Scaled}$ is large when the AMM of quarks

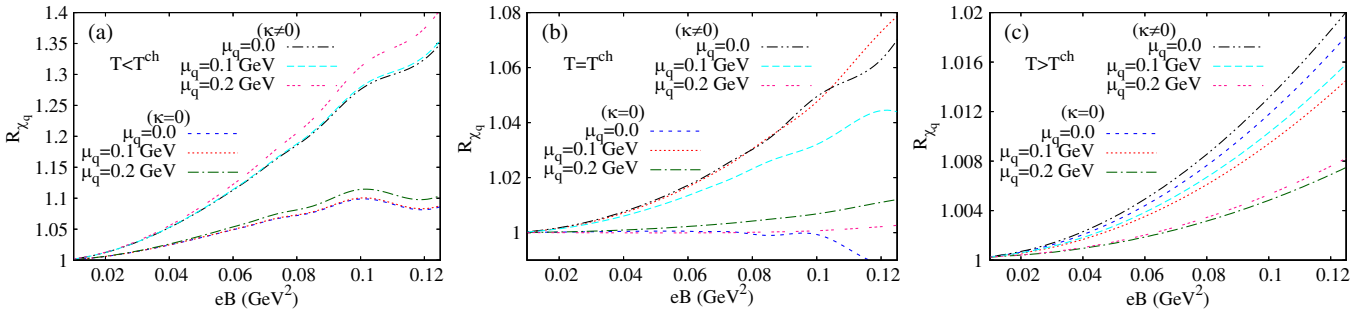

FIG. 4. R_{χ_q} as a function of eB for various values of μ_q with and without AMM at (a) chiral broken phase, (b) in the vicinity of chiral phase transition for $\mu_q = 0$, $eB = 0$, (c) partial chiral restored phase.

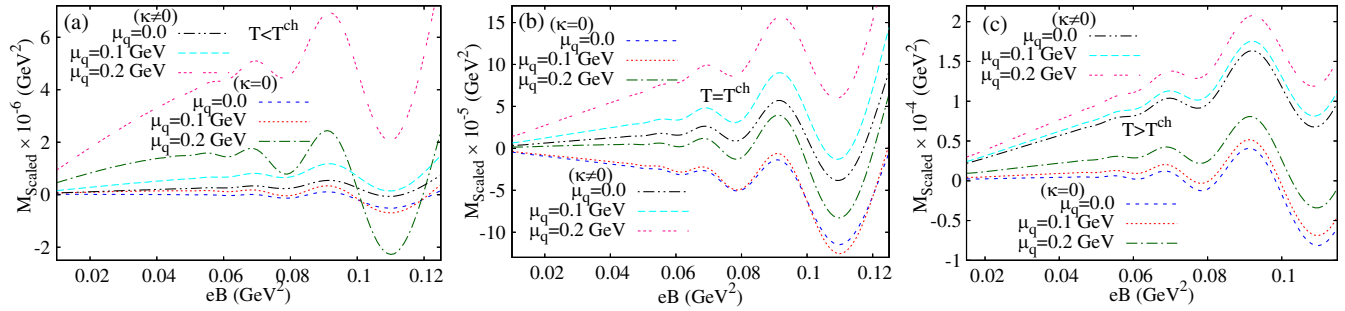

FIG. 5. Scaled magnetization ($\mathcal{M}_{\text{Scaled}}$) as a function of eB for various values of μ_q at (a) chiral broken phase, (b) in the vicinity of chiral phase transition, (c) partial chiral restored phase.

is considered [black and blue lines in any of the subplots of Figs. 5(a)–5(c)].

D. Speed of sound at constant s/n_B

In this subsection, we study the variation of speed of sound with temperature in presence of a background magnetic field in quark matter. As discussed in Sec. III, c^2_{s/n_q} splits into $c^{2(\parallel)}_{s/n_q}$ and $c^{2(\perp)}_{s/n_q}$ along and perpendicular to the direction of the background magnetic field, respectively. We use Eqs. (28) and (29) to determine the speed of sound.

Figure 6(a) illustrates the variation of $c^{2(\parallel)}_{s/n_q}$ as a function of temperature for various values of μ_q at $eB = 0.10$ GeV^2 both with and without AMM of quarks. In all the plots, $c^{2(\parallel)}_{s/n_q}$ decreases initially with temperature, reaches its lowest value, then sharply increases over a short temperature range before saturating slightly below the ideal gas value. This minimum value, known as the softest point, may be an important indicator of the transitions observed in heavy-ion collisions [111]. Following a transition or crossover, the release of new degrees of freedom leads to a rapid increase in the speed of sound. In all plots, this transition point shifts towards lower temperatures with increasing μ_q [green, blue, and red lines in Fig. 6(a)]. Conversely, the magnitude of $c^{2(\parallel)}_{s/n_q}$ decreases with the increase of μ_q below the transition temperature. However, $c^{2(\parallel)}_{s/n_q}$ increases with the increase of μ_q above the transition temperature. The figure also shows that near the transition region the plots shift towards lower T values with the inclusion of AMM of quarks [red and cyan lines in Fig. 6(a)] but the behavior of the speed of sound remains same as observed without AMM of quarks. Similarly, Fig. 6(b) presents the variation of $c^{2(\perp)}_{s/n_q}$ as a function of temperature for various values of μ_q at $eB = 0.10$ GeV^2 considering both with and without AMM of quarks. The qualitative behavior of $c^{2(\perp)}_{s/n_q}$ is same as $c^{2(\parallel)}_{s/n_q}$. With the inclusion of AMM of quarks Fig. 6(b) shows that the magnitude of $c^{2(\perp)}_{s/n_q}$ decreases more for a given value of μ_q at lower temperature region [black and blue lines in Fig. 6(b)] which is opposite to the behavior of $c^{2(\parallel)}_{s/n_q}$ observed in Fig. 6(a). Additionally, the lowest value of $c^{2(\perp)}_{s/n_q}$ decreases due to AMM of quarks [red and cyan lines in Fig. 6(b)]. The comparison between the parallel and perpendicular components of c^2_{s/n_q} as a function of temperature at $eB = 0.1$ GeV^2 and $\mu_q = 0.2$ GeV is presented in Fig. 6(c). Notably, there is a significant difference between the components. In the absence of AMM of quarks, $c^{2(\perp)}_{s/n_q}$

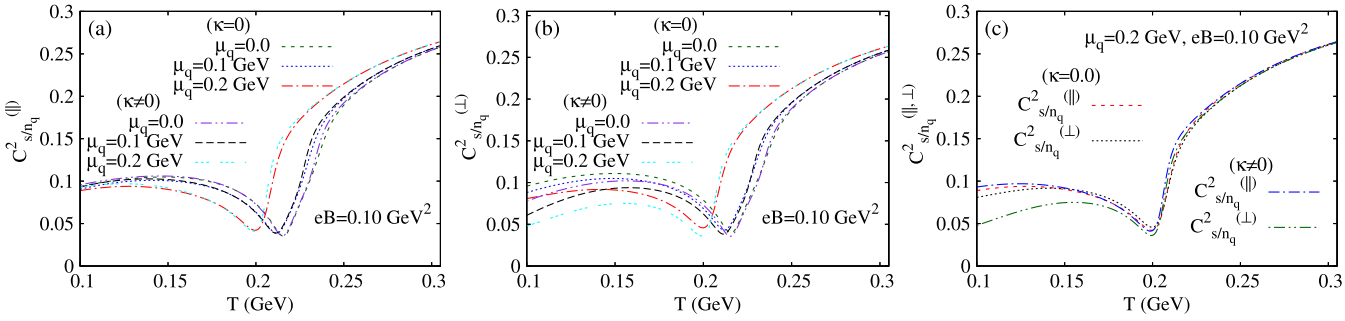

FIG. 6. (a) $C^{2(\parallel)}_{s/n_B}$ and (b) $C^{2(\perp)}_{s/n_B}$ as a function of T for various values of $\mu_q = 0, 0.1, 0.2$ GeV at $eB = 0.10$ GeV^2, (c) $C^{2(\parallel,\perp)}_{s/n_B}$ as a function of T at $\mu_q = 0.2$ GeV and $eB = 0.10$ GeV^2.

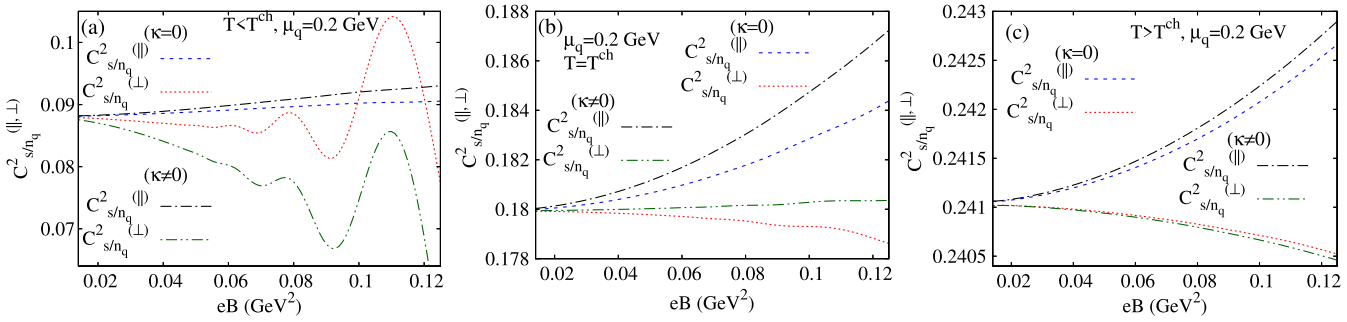

FIG. 7. $c_{s/n_q}^{2(\parallel,\perp)}$ as a function of eB for $\mu_q = 0.2$ GeV with and without AMM of quark at (a) chiral broken phase, (b) in the vicinity of chiral phase transition, (c) partial chiral restored phase.

follows a similar trend. However, in the presence of the AMM of quarks, $c_{s/n_q}^{2(\parallel)}$ is greater than $c_{s/n_q}^{2(\perp)}$ in the symmetry broken phase [blue and green lines in Fig. 6(c)].

Next, we will discuss the variation of $c_{s/n_q}^{2(\parallel,\perp)}$ as a function of the background magnetic field for different values of μ_q both with and without AMM of quarks at different stages of chiral phase transition as mentioned previously in Sec. IV A. Figures 7(a)–7(c) represent speed of sound in the chirally broken phase ($T < T^{\rm ch}$), near chiral phase transition ($T \simeq T^{\rm ch}$) and partial chirally restored phase ($T > T^{\rm ch}$), respectively. For both with and without AMM of quarks, Fig. 7(a) shows that $c_{s/n_q}^{2(\parallel)}$ increases while $c_{s/n_q}^{2(\perp)}$ oscillates with increasing background magnetic field. Around the chiral phase transition, Fig. 7(b) shows that the oscillations in $c_{s/n_q}^{2(\perp)}$ has disappeared. However, in the partially chiral restored phase as shown in Fig. 7(c), $c_{s/n_q}^{2(\parallel)}$ increases and $c_{s/n_q}^{2(\perp)}$ decreases smoothly with increasing eB. Finally, in both the chirally broken and partially chiral restored phase, $c_{s/n_q}^{2(\parallel)}$ increases more and $c_{s/n_q}^{2(\perp)}$ decreases more with the increase of the background magnetic field when AMM of quarks is included.

E. Isothermal compressibility

The isothermal compressibility (K_T) remains isotropic in all directions when there is no magnetic field present. Consequently, the EOS is the same across all directions. However, K_T exhibits anisotropic behavior and splits into $K_T^{\parallel,\perp}$ along and perpendicular to the direction of background magnetic field, respectively. We use Eqs. (31)–(32) to calculate isothermal compressibility. Figure 8(a) illustrates $K_T^{\parallel,\perp}$ as a function of temperature at $eB = 0.10$ GeV^2 and $\mu_q = 0.2$ GeV considering both scenarios with and without the AMM of quarks. In both cases, $K_T^{\parallel,\perp}$ decrease as temperature increases. This suggests that QCD matter becomes highly incompressible with increasing temperature irrespective of directions. With the inclusion of the AMM of quarks, $K_T^{\perp}$ is greater than $K_T^{\parallel}$ [green and black lines in inset plot of Fig. 8(a)] and the difference between $K_T^{\parallel}$ and $K_T^{\perp}$ decreases with increasing temperature. Therefore, the EOS becomes less stiff along the field direction compared to other directions when the AMM of quarks is considered and $K_T^{\parallel,\perp}$ becomes nearly isotropic at very high temperature. Conversely, the difference between $K_T^{\parallel}$ and $K_T^{\perp}$ is very small without AMM of quarks [blue and red lines in inset plot of Fig. 8(a)]. Moreover, plots in the figure clearly indicate a crossover or transition occurring around $T \simeq 205$ MeV that can be connected to the observation in Fig. 3(b).

Next, we present $K_T^{\parallel,\perp}$ as a function eB for $\mu_q = 0.2$ GeV both with and without the AMM of quarks at various stages of chiral phase transition as mentioned previously in Sec. IV A. Figures 9(a)–9(c) represent chirally broken phase, near the chiral phase transition and partially restored phase, respectively. In Fig. 9(a), $K_T^{\perp}$ exhibits oscillations with increasing background magnetic fields and its values are higher indicating more compressible QCD matter when considering the AMM of quark [red and green lines in Fig. 9(a)]. Conversely, $K_T^{\parallel}$ decreases with

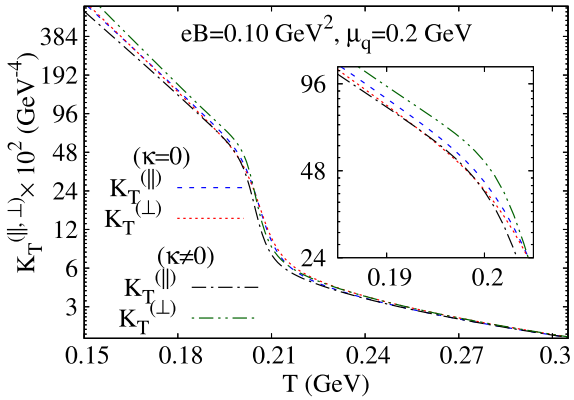

FIG. 8. $K_T^{(\parallel,\perp)}$ as a function of T at $\mu_q = 0.2$ GeV and $eB = 0.10$ GeV^2 with and without AMM of quarks.

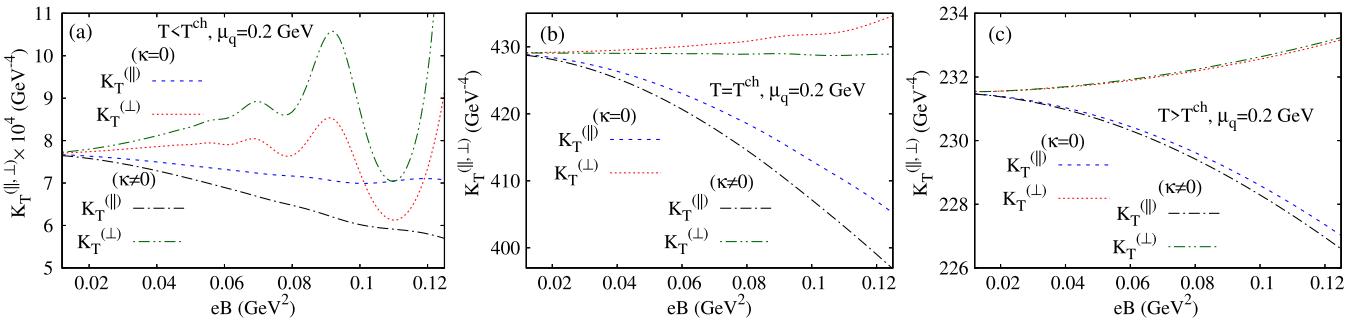

FIG. 9. $K_T^{(\parallel,\perp)}$ as a function of eB for $\mu_q = 0.2$ GeV with and without AMM of quark at (a) chiral broken phase, (b) near chiral phase transition, (c) partial chiral restored phase.

increasing background magnetic fields [blue and black lines in Fig. 9(a)] reflecting a lower compressibility in the presence of the AMM of quarks. Figure 9(b) reveals that without the AMM of quarks, $K_T^{\perp}$ increases more with increasing eB unlike the scenario with the inclusion of the AMM of quarks [red and green lines in Fig. 9(b)]. On the other hand, $K_T^{\parallel}$ decreases with increasing background magnetic field and its decreasing nature is larger in the presence of the AMM of quarks [blue and black lines in Fig. 9(a)]. Moreover, Fig. 9(c) indicates an increase in $K_T^{\perp}$ [red line in Fig. 9(c)] and a decrease in $K_T^{\parallel}$ [blue line in Fig. 9(c)] with rising magnetic fields. These changes are more prominent when the AMM of quarks is taken into account [black and blue lines in Fig. 9(c)].

V. SUMMARY AND CONCLUSION

In summary, we have investigated several properties of quark matter subjected to a background magnetic field both with and without the AMM of quarks at finite temperature and chemical potential within the framework of the PNJL model. The study involves the constituent quark mass, quark number density, and quark number susceptibility (normalized by its value at zero or weak magnetic field), as well as the speed of sound and isothermal compressibility.

The constituent quark mass initially starts at a high value and remains relatively stable at lower temperatures indicating a chirally broken phase. However, it decreases rapidly within a narrow temperature range and eventually approaches the bare mass of quarks indicating partial restoration of chiral symmetry. This transition typically occurs around $T^{\rm ch} \sim 230$ MeV in a scenario without the magnetic field and zero chemical potential. In the chirally broken phase, we observe an increasing trend in the quark mass as the magnetic field strength rises, a phenomenon known as MC. Conversely, when the AMM of quarks is considered, we observe an opposite trend referred to as IMC.

Additionally, we have observed a suppression in the quark number density at low temperatures attributed to the effective interactions of the gluon field. These interactions restrict contributions from both the one-quark and two-quark states. However, this suppression becomes less pronounced at higher temperatures.

It is observed that the presence of a background magnetic field tends to shift the transition temperature ($T_c^{\chi_q}$) to higher values indicating MC. On the contrary, inclusion of AMM of quarks decreases the transition temperature confirming that IMC observed by analysing the results of gap equations. The susceptibility normalized by its value at zero or weak magnetic field is an important probe for studying magnetic fields observed in noncentral HICs.

Our study reveals that the presence of a magnetic field induces anisotropy in the speed of sound leading to variations between the $c^{2}_{s/n_q}{}^{(\parallel,\perp)}$ components. Notably, the qualitative behavior of $c^{2(\perp)}_{s/n_q}$ is similar to that of $c^{2(\parallel)}_{s/n_q}$. When the AMM of quarks is included, we find that the magnitude of $c^{2(\perp)}_{s/n_q}$ decreases more for a given value of μ_q in the lower temperature region, opposite to the behavior of $c^{2(\parallel)}_{s/n_q}$.

In the presence of the magnetic field, the isothermal compressibility also becomes anisotropic dividing into $K_T^{\parallel,\perp}$ along and perpendicular to the direction of magnetic field. The $K_T^{\parallel,\perp}$ decrease as temperature rises indicating a trend towards increased incompressibility of QCD matter regardless of its orientation with respect to the direction of magnetic field. Upon considering AMM of quarks, $K_T^{\perp}$ is greater than $K_T^{\parallel}$, and the difference between $K_T^{\parallel,\perp}$ decreases with increasing temperature. Therefore, the EOS becomes more stiff along the field direction compared to other directions and becomes nearly isotropic at very high temperature. On the other hand, $K_T^{\parallel}$ decreases and $K_T^{\perp}$ increases with increasing background magnetic field. Hence, the system is less compressible along the magnetic field direction with increasing background magnetic field.

APPENDIX A: MATHEMATICAL DETAILS

$$\frac{\partial f_\Lambda}{\partial B} = -\frac{N(2n+1-s)\Lambda^{2N}P_{nfs}^{2(N-1)}}{(\Lambda^{2N}+P_{nfs}^{2N})^2}|e_f|, \qquad P_{nfs} = \sqrt{p_z^2+(2n+1-s)|e_fB|}, \tag{A1}$$

$$\frac{\partial \omega_{nfs}}{\partial M} = \frac{M}{\omega_{nfs}}\left(1-\frac{sk_fe_fB}{M_{nfs}}\right), \qquad \frac{\partial M_{nfs}}{\partial M} = \frac{M}{M_{nfs}}, \tag{A2}$$

$$\frac{\partial \ln g^+}{\partial T} = \left(\frac{\partial \ln g^+}{\partial M}\right)\frac{\partial M}{\partial T} + \left(\frac{\partial \ln g^+}{\partial \Phi}\right)\frac{\partial \Phi}{\partial T} + \left(\frac{\partial \ln g^+}{\partial \bar{\Phi}}\right)\frac{\partial \bar{\Phi}}{\partial T} + \left(\frac{\partial \ln g^+}{\partial T}\right)_{M,\Phi,\bar{\Phi}}, \tag{A3}$$

$$\frac{\partial \ln g^+}{\partial \mu_q} = \left(\frac{\partial \ln g^+}{\partial M}\right)\frac{\partial M}{\partial \mu_q} + \left(\frac{\partial \ln g^+}{\partial \Phi}\right)\frac{\partial \Phi}{\partial \mu_q} + \left(\frac{\partial \ln g^+}{\partial \bar{\Phi}}\right)\frac{\partial \bar{\Phi}}{\partial \mu_q} + \left(\frac{\partial \ln g^+}{\partial \mu_q}\right)_{M,\Phi,\bar{\Phi}}, \tag{A4}$$

$$\frac{\partial \ln g^+}{\partial M} = -3\beta\frac{\partial \omega_{nfs}}{\partial M}f^+, \quad \frac{\partial \ln g^+}{\partial \Phi} = \frac{3e^{-\beta(\omega_{nfs}-\mu_q)}}{g^+}, \quad \frac{\partial \ln g^+}{\partial \bar{\Phi}} = \frac{3e^{-2\beta(\omega_{nfs}-\mu_q)}}{g^+}, \qquad \left(\frac{\partial \ln g^+}{\partial \mu_q}\right)_{M,\Phi,\bar{\Phi}} = 3\beta f^+, \tag{A5}$$

$$\left(\frac{\partial \ln g^+}{\partial T}\right)_{M,\Phi,\bar{\Phi}} = \frac{\omega_{nfs}-\mu_q}{T^2}3f^+, \tag{A6}$$

$$\frac{\partial \ln g^-}{\partial T} = \left(\frac{\partial \ln g^-}{\partial M}\right)\frac{\partial M}{\partial T} + \left(\frac{\partial \ln g^-}{\partial \Phi}\right)\frac{\partial \Phi}{\partial T} + \left(\frac{\partial \ln g^-}{\partial \bar{\Phi}}\right)\frac{\partial \bar{\Phi}}{\partial T} + \left(\frac{\partial \ln g^-}{\partial T}\right)_{M,\Phi,\bar{\Phi}}, \tag{A7}$$

$$\frac{\partial \ln g^-}{\partial \mu_q} = \left(\frac{\partial \ln g^-}{\partial M}\right)\frac{\partial M}{\partial \mu_q} + \left(\frac{\partial \ln g^-}{\partial \Phi}\right)\frac{\partial \Phi}{\partial \mu_q} + \left(\frac{\partial \ln g^-}{\partial \bar{\Phi}}\right)\frac{\partial \bar{\Phi}}{\partial \mu_q} + \left(\frac{\partial \ln g^-}{\partial \mu_q}\right)_{M,\Phi,\bar{\Phi}}, \tag{A8}$$

$$\frac{\partial \ln g^-}{\partial M} = -3\beta\frac{\partial \omega_{nfs}}{\partial M}f^-, \quad \frac{\partial \ln g^-}{\partial \Phi} = \frac{3e^{-2\beta(\omega_{nfs}+\mu_q)}}{g^-}, \quad \frac{\partial \ln g^-}{\partial \bar{\Phi}} = \frac{3e^{-\beta(\omega_{nfs}+\mu_q)}}{g^-}, \qquad \left(\frac{\partial \ln g^-}{\partial \mu_q}\right)_{M,\Phi,\bar{\Phi}} = -3\beta f^-, \tag{A9}$$

$$\left(\frac{\partial \ln g^-}{\partial T}\right)_{M,\Phi,\bar{\Phi}} = \frac{\omega_{nfs}+\mu_q}{T^2}3f^-, \tag{A10}$$

$$\frac{\partial f^+}{\partial T} = \left(\frac{\partial f^+}{\partial M}\right)\frac{\partial M}{\partial T} + \left(\frac{\partial f^+}{\partial \Phi}\right)\frac{\partial \Phi}{\partial T} + \left(\frac{\partial f^+}{\partial \bar{\Phi}}\right)\frac{\partial \bar{\Phi}}{\partial T} + \left(\frac{\partial f^+}{\partial T}\right)_{M,\Phi,\bar{\Phi}}, \tag{A11}$$

$$\frac{\partial f^+}{\partial \mu_q} = \left(\frac{\partial f^+}{\partial M}\right)\frac{\partial M}{\partial \mu_q} + \left(\frac{\partial f^+}{\partial \Phi}\right)\frac{\partial \Phi}{\partial \mu_q} + \left(\frac{\partial f^+}{\partial \bar{\Phi}}\right)\frac{\partial \bar{\Phi}}{\partial \mu_q} + \left(\frac{\partial f^+}{\partial \mu_q}\right)_{M,\Phi,\bar{\Phi}}, \tag{A12}$$

$$\frac{\partial f^+}{\partial M} = \beta\frac{\partial \omega_{nfs}}{\partial M}\left[3f^{+2} - \frac{1}{g^+}\left[\{\Phi+4\bar{\Phi}e^{-\beta(\omega_{nfs}-\mu_q)}\}e^{-\beta(\omega_{nfs}-\mu_q)} + 3e^{-3\beta(\omega_{nfs}-\mu_q)}\right]\right], \tag{A13}$$

$$\frac{\partial f^+}{\partial \Phi} = \frac{1-3f^+}{g^+}e^{-\beta(\omega_{nfs}-\mu_q)}, \qquad \frac{\partial f^+}{\partial \bar{\Phi}} = \frac{2-3f^+}{g^+}e^{-2\beta(\omega_{nfs}-\mu_q)}, \tag{A14}$$

$$\left(\frac{\partial f^+}{\partial \mu_q}\right)_{M,\Phi,\bar{\Phi}} = \beta\left[\frac{1}{g^+}\{(\Phi+4\bar{\Phi}e^{-\beta(\omega_{nfs}-\mu_q)})e^{-\beta(\omega_{nfs}-\mu_q)} + 3e^{-3\beta(\omega_{nfs}-\mu_q)}\} - 3f^{+2}\right], \tag{A15}$$

$$\left(\frac{\partial f^+}{\partial T}\right)_{M,\Phi,\bar{\Phi}} = \frac{\omega_{nfs}-\mu_q}{T^2}\left[\frac{1}{g^+}\{(\Phi+4\bar{\Phi}e^{-\beta(\omega_{nfs}-\mu_q)})e^{-\beta(\omega_{nfs}-\mu_q)} + 3e^{-3\beta(\omega_{nfs}-\mu_q)}\} - 3f^{+2}\right], \tag{A16}$$

$$\frac{\partial f^-}{\partial T} = \left(\frac{\partial f^-}{\partial M}\right)\frac{\partial M}{\partial T} + \left(\frac{\partial f^-}{\partial \Phi}\right)\frac{\partial \Phi}{\partial T} + \left(\frac{\partial f^-}{\partial \bar{\Phi}}\right)\frac{\partial \bar{\Phi}}{\partial T} + \left(\frac{\partial f^-}{\partial T}\right)_{M,\Phi,\bar{\Phi}}, \tag{A17}$$

$$\frac{\partial f^-}{\partial \mu_q} = \left(\frac{\partial f^-}{\partial M}\right)\frac{\partial M}{\partial \mu_q} + \left(\frac{\partial f^-}{\partial \Phi}\right)\frac{\partial \Phi}{\partial \mu_q} + \left(\frac{\partial f^-}{\partial \bar{\Phi}}\right)\frac{\partial \bar{\Phi}}{\partial \mu_q} + \left(\frac{\partial f^-}{\partial \mu_q}\right)_{M,\Phi,\bar{\Phi}}, \tag{A18}$$

$$\frac{\partial f^-}{\partial M} = \frac{\partial f^+}{\partial M}(\Phi \to \bar{\Phi}, \mu_q \to -\mu_q), \qquad \frac{\partial f^-}{\partial \Phi} = \frac{2-3f^-}{g^-}e^{-2\beta(\omega_{nfs}+\mu_q)}, \qquad \frac{\partial f^-}{\partial \bar{\Phi}} = \frac{1-3f^-}{g^-}e^{-\beta(\omega_{nfs}+\mu_q)}, \tag{A19}$$

$$\left(\frac{\partial f^-}{\partial \mu_q}\right)_{M,\Phi,\bar{\Phi}} = -\beta\left[\frac{1}{g^-}\{(\bar{\Phi}+4\Phi e^{-\beta(\omega_{nfs}+\mu_q)})e^{-\beta(\omega_{nfs}+\mu_q)} + 3e^{-3\beta(\omega_{nfs}+\mu_q)}\} - 3(f^-)^2\right], \tag{A20}$$

$$\left(\frac{\partial f^-}{\partial T}\right)_{M,\Phi,\bar{\Phi}} = \left(\frac{\partial f^+}{\partial \mu_q}\right)_{M,\Phi,\bar{\Phi}}(\Phi \to \bar{\Phi}, \mu_q \to -\mu_q). \tag{A21}$$

APPENDIX B: THERMODYNAMICAL RELATIONS

$$\left(\frac{\partial(s/n_q)}{\partial \mu_q}\right)_T = \frac{1}{n_q}\left(\frac{\partial s}{\partial \mu_q}\right)_T - \frac{s}{n_q^2}\left(\frac{\partial n_q}{\partial \mu_q}\right)_T, \qquad \left(\frac{\partial(s/n_q)}{\partial T}\right)_{\mu_q} = \frac{1}{n_q}\left(\frac{\partial s}{\partial T}\right)_T - \frac{s}{n_q^2}\left(\frac{\partial n_q}{\partial T}\right)_{\mu_q}, \tag{B1}$$

$$\left(\frac{\partial \epsilon}{\partial T}\right)_{\mu_q} = T\left(\frac{\partial s}{\partial T}\right)_{\mu_q} + \mu_q\left(\frac{\partial n_q}{\partial T}\right)_{\mu_q}, \qquad \left(\frac{\partial \epsilon}{\partial \mu_q}\right)_T = T\left(\frac{\partial s}{\partial \mu_q}\right)_T + \mu_q\left(\frac{\partial n_q}{\partial \mu_q}\right)_T. \tag{B2}$$

APPENDIX C: SUSCEPTIBILITIES

In Sec. III, we have observed that the speed of sound, isothermal compressibility in Eqs. (26)–(32) involve the partial derivatives $(\frac{\partial \mathcal{M}}{\partial T})_{\mu_q}$, $(\frac{\partial \mathcal{M}}{\partial \mu_q})_T$, $(\frac{\partial s}{\partial \mu_q})_T$, $(\frac{\partial s}{\partial T})_{\mu_q}$, $(\frac{\partial n_q}{\partial \mu_q})_T$, and $(\frac{\partial n_q}{\partial T})_{\mu_q}$, which can be derived from the free energy. The expressions are provided below:

$$\begin{aligned}
\left(\frac{\partial \mathcal{M}}{\partial T}\right)_{\mu_q} &= 3\sum_{nfs}\frac{|e_f|}{2\pi}\int_{-\infty}^{+\infty}\frac{dp_z}{2\pi}f_\Lambda\frac{\partial \omega_{nfs}}{\partial M}\frac{\partial M}{\partial T} + 3\sum_{nfs}\frac{|e_fB|}{2\pi}\int_{-\infty}^{+\infty}\frac{dp_z}{2\pi}\frac{\partial f_\Lambda}{\partial B}\frac{\partial \omega_{nfs}}{\partial M}\frac{\partial M}{\partial T} \\
&+ \sum_{nfs}\frac{|e_f|}{2\pi}\int_{-\infty}^{+\infty}\frac{dp_z}{2\pi}\{\ln g^+ + \ln g^-\} + T\sum_{nfs}\frac{|e_f|}{2\pi}\int_{-\infty}^{+\infty}\frac{dp_z}{2\pi}\left\{\frac{\partial \ln g^+}{\partial T} + \frac{\partial \ln g^-}{\partial T}\right\} \\
&+ 3\sum_{nfs}\frac{|e_fB|}{2\pi}\int_{-\infty}^{+\infty}\frac{dp_z}{2\pi}\frac{-1}{\omega_{nfs}^2}\frac{\partial \omega_{nfs}}{\partial M}\frac{\partial M}{\partial T}\left\{1-\frac{s\kappa_f e_f B}{M_{nfs}}\right\}\left\{\frac{2n+1-s}{2}|e_f| - s\kappa_f e_f M_{nfs}\right\}\{f_\Lambda - f^+ - f^-\} \\
&+ 3\sum_{nfs}\frac{|e_fB|}{2\pi}\int_{-\infty}^{+\infty}\frac{dp_z}{2\pi}\frac{1}{\omega_{nfs}}\left\{-s\kappa_f e_f B\left(\frac{-M}{M_{nfs}^3}\right)\frac{\partial M}{\partial T}\right\}\left\{\frac{2n+1-s}{2}|e_f| - s\kappa_f e_f M_{nfs}\right\}\{f_\Lambda - f^+ - f^-\} \\
&+ 3\sum_{nfs}\frac{|e_fB|}{2\pi}\int_{-\infty}^{+\infty}\frac{dp_z}{2\pi}\frac{1}{\omega_{nfs}}\left\{1-\frac{s\kappa_f e_f B}{M_{nfs}}\right\}\left(-s\kappa_f e_f\left(\frac{M}{M_{nfs}}\right)\frac{\partial M}{\partial T}\right)\{f_\Lambda - f^+ - f^-\} \\
&+ 3\sum_{nfs}\frac{|e_fB|}{2\pi}\int_{-\infty}^{+\infty}\frac{dp_z}{2\pi}\frac{1}{\omega_{nfs}}\left\{1-\frac{s\kappa_f e_f B}{M_{nfs}}\right\}\left\{\frac{2n+1-s}{2}|e_f| - s\kappa_f e_f M_{nfs}\right\}\left\{-\frac{\partial f^+}{\partial T} - \frac{\partial f^-}{\partial T}\right\},
\end{aligned} \tag{C1}$$

$$\left(\frac{\partial\mathcal{M}}{\partial\mu_q}\right)_T = 3\sum_{nfs}\frac{|e_f|}{2\pi}\int_{-\infty}^{+\infty}\frac{dp_z}{2\pi}f_\Lambda\frac{\partial\omega_{nfs}}{\partial M}\frac{\partial M}{\partial\mu_q}+3\sum_{nfs}\frac{|e_fB|}{2\pi}\int_{-\infty}^{+\infty}\frac{dp_z}{2\pi}\frac{\partial f_\Lambda}{\partial B}\frac{\partial\omega_{nfs}}{\partial M}\frac{\partial M}{\partial\mu_q}+T\sum_{nfs}\frac{|e_f|}{2\pi}\int_{-\infty}^{+\infty}\frac{dp_z}{2\pi}\left\{\frac{\partial\ln g^+}{\partial\mu_q}+\frac{\partial\ln g^-}{\partial\mu_q}\right\}$$
$$+3\sum_{nfs}\frac{|e_fB|}{2\pi}\int_{-\infty}^{+\infty}\frac{dp_z}{2\pi}\frac{-1}{\omega_{nfs}^2}\frac{\partial\omega_{nfs}}{\partial M}\frac{\partial M}{\partial\mu_q}\left\{1-\frac{s\kappa_f e_f B}{M_{nfs}}\right\}\left\{\frac{2n+1-s}{2}|e_f|-s\kappa_f e_f M_{nfs}\right\}\{f_\Lambda-f^+-f^-\}$$
$$+3\sum_{nfs}\frac{|e_fB|}{2\pi}\int_{-\infty}^{+\infty}\frac{dp_z}{2\pi}\frac{1}{\omega_{nfs}}\left\{-s\kappa_f e_f B\left(\frac{-M}{M_{nfs}^3}\right)\frac{\partial M}{\partial\mu_q}\right\}\left\{\frac{2n+1-s}{2}|e_f|-s\kappa_f e_f M_{nfs}\right\}\{f_\Lambda-f^+-f^-\}$$
$$+3\sum_{nfs}\frac{|e_fB|}{2\pi}\int_{-\infty}^{+\infty}\frac{dp_z}{2\pi}\frac{1}{\omega_{nfs}}\left\{1-\frac{s\kappa_f e_f B}{M_{nfs}}\right\}\left\{-s\kappa_f e_f\left(\frac{M}{M_{nfs}}\right)\frac{\partial M}{\partial\mu_q}\right\}\{f_\Lambda-f^+-f^-\}$$
$$+3\sum_{nfs}\frac{|e_fB|}{2\pi}\int_{-\infty}^{+\infty}\frac{dp_z}{2\pi}\frac{1}{\omega_{nfs}}\left\{1-\frac{s\kappa_f e_f B}{M_{nfs}}\right\}\left\{\frac{2n+1-s}{2}|e_f|-s\kappa_f e_f M_{nfs}\right\}\left\{-\frac{\partial f^+}{\partial\mu_q}-\frac{\partial f^-}{\partial\mu_q}\right\}, \tag{C2}$$

$$\left(\frac{\partial s}{\partial T}\right)_{\mu_q} = \frac{\partial s_0}{\partial T}+\sum_{nfs}\frac{|e_fB|}{2\pi}\int_{-\infty}^{+\infty}\frac{dp_z}{2\pi}\left\{\frac{\partial\ln g^+}{\partial T}+\frac{\partial\ln g^-}{\partial T}\right\}+3\sum_{nfs}\frac{|e_fB|}{2\pi}\int_{-\infty}^{+\infty}\frac{dp_z}{2\pi}\left\{\frac{\omega_{nfs}-\mu_q}{T}\frac{\partial f^+}{\partial T}+\frac{\omega_{nfs}+\mu_q}{T}\frac{\partial f^-}{\partial T}\right\}$$
$$+3\sum_{nfs}\frac{|e_fB|}{2\pi}\int_{-\infty}^{+\infty}\frac{dp_z}{2\pi}\left\{\left(\frac{\omega_{nfs}-\mu_q}{-T^2}+\frac{1}{T}\frac{\partial\omega_{nfs}}{\partial M}\frac{\partial M}{\partial T}\right)f^+ + \left(\frac{\omega_{nfs}+\mu_q}{-T^2}+\frac{1}{T}\frac{\partial\omega_{nfs}}{\partial M}\frac{\partial M}{\partial T}\right)f^-\right\}, \tag{C3}$$

$$\left(\frac{\partial s}{\partial\mu_q}\right)_T = \frac{\partial s_0}{\partial\mu_q}+\sum_{nfs}\frac{|e_fB|}{2\pi}\int_{-\infty}^{+\infty}\frac{dp_z}{2\pi}\left\{\frac{\partial\ln g^+}{\partial\mu_q}+\frac{\partial\ln g^-}{\partial\mu_q}\right\}+3\sum_{nfs}\frac{|e_fB|}{2\pi}\int_{-\infty}^{+\infty}\frac{dp_z}{2\pi}\left\{\frac{\omega_{nfs}-\mu_q}{T}\frac{\partial f^+}{\partial\mu_q}+\frac{\omega_{nfs}+\mu_q}{T}\frac{\partial f^-}{\partial\mu_q}\right\}$$
$$+3\sum_{nfs}\frac{|e_fB|}{2\pi}\int_{-\infty}^{+\infty}\frac{dp_z}{2\pi}\left\{\left(\frac{\omega_{nfs}-\mu_q}{-T^2}+\frac{1}{T}\frac{\partial\omega_{nfs}}{\partial M}\frac{\partial M}{\partial\mu_q}\right)f^+ + \left(\frac{\omega_{nfs}+\mu_q}{-T^2}+\frac{1}{T}\frac{\partial\omega_{nfs}}{\partial M}\frac{\partial M}{\partial\mu_q}\right)f^-\right\}, \tag{C4}$$

$$\left(\frac{\partial n_q}{\partial T}\right)_{\mu_q} = 3\sum_{nfs}\frac{|e_fB|}{2\pi}\int_{-\infty}^{+\infty}\frac{dp_z}{2\pi}\left(\frac{\partial f^+}{\partial T}-\frac{\partial f^-}{\partial T}\right), \tag{C5}$$

$$\left(\frac{\partial n_q}{\partial\mu_q}\right)_T = 3\sum_{nfs}\frac{|e_fB|}{2\pi}\int_{-\infty}^{+\infty}\frac{dp_z}{2\pi}\left(\frac{\partial f^+}{\partial\mu_q}-\frac{\partial f^-}{\partial\mu_q}\right). \tag{C6}$$

The partial derivaties—$\frac{\partial M}{\partial T}$, $\frac{\partial\phi}{\partial T}$, $\frac{\partial\bar{\phi}}{\partial T}$ and $\frac{\partial M}{\partial\mu_q}$, $\frac{\partial\phi}{\partial\mu_q}$, $\frac{\partial\bar{\phi}}{\partial\mu_q}$—involved in previous equations can be obtained from the coupled Eqs. (11)–(13). We define X, Y, Z using the gap Eqs. (11)–(13) as

$$X = (M-m)-6G\sum_{nfs}\frac{|e_fB|}{2\pi}\int_{-\infty}^{+\infty}\frac{dp_z}{2\pi}\frac{1}{\omega_{nfs}}\frac{M}{M_{nfs}}\{M_{nfs}-s\kappa_f e_f B\}(1-f^+-f^-), \tag{C7}$$

$$Y = \frac{\partial U}{\partial\Phi}-3T\sum_{nfs}\frac{|e_fB|}{2\pi}\int_{-\infty}^{+\infty}\frac{dp_z}{2\pi}\left\{\frac{e^{-\frac{\omega_{nfs}-\mu_q}{T}}}{g^+}+\frac{e^{-2\frac{\omega_{nfs}+\mu_q}{T}}}{g^-}\right\}, \tag{C8}$$

$$Z = \frac{\partial U}{\partial\bar{\Phi}}-3T\sum_{nfs}\frac{|e_fB|}{2\pi}\int_{-\infty}^{+\infty}\frac{dp_z}{2\pi}\left\{\frac{e^{-2\frac{\omega_{nfs}-\mu_q}{T}}}{g^+}+\frac{e^{-\frac{\omega_{nfs}+\mu_q}{T}}}{g^-}\right\}. \tag{C9}$$

Taking derivative with respect to temperature and chemical potential, the Eqs. (C7)–(C9) can be expressed in the matrix form as

$$\begin{pmatrix} X_M & X_\phi & X_{\bar{\Phi}} \\ Y_M & Y_\phi & Y_{\bar{\Phi}} \\ Z_M & Z_\phi & Z_{\bar{\Phi}} \end{pmatrix} \begin{pmatrix} \frac{\partial M}{\partial T} \\ \frac{\partial \phi}{\partial T} \\ \frac{\partial \bar{\phi}}{\partial T} \end{pmatrix} = \begin{pmatrix} X_T \\ Y_T \\ Z_T \end{pmatrix}, \tag{C10}$$

$$\begin{pmatrix} X_M & X_\phi & X_{\bar{\Phi}} \\ Y_M & Y_\phi & Y_{\bar{\Phi}} \\ Z_M & Z_\phi & Z_{\bar{\Phi}} \end{pmatrix} \begin{pmatrix} \frac{\partial M}{\partial \mu_q} \\ \frac{\partial \phi}{\partial \mu_q} \\ \frac{\partial \bar{\phi}}{\partial \mu_q} \end{pmatrix} = \begin{pmatrix} X_{\mu_q} \\ Y_{\mu_q} \\ Z_{\mu_q} \end{pmatrix}, \tag{C11}$$

where

$$X_M = 1 - 6G\sum_{nfs}\frac{|e_f B|}{2\pi}\int_{-\infty}^{+\infty}\frac{dp_z}{2\pi}\left[\left\{\frac{1}{\omega_{nfs}}\frac{1}{M_{nfs}} - \frac{1}{\omega_{nfs}^2}\frac{M}{M_{nfs}}\frac{\partial\omega_{nfs}}{\partial M} - \frac{1}{\omega_{nfs}}\frac{M^2}{M_{nfs}^3}\right\}(M_{nfs} - s\kappa_f e_f B)(1 - f^+ - f^-)\right.$$
$$\left. + \frac{1}{\omega_{nfs}}\left(\frac{M}{M_{nfs}}\right)^2(1 - f^+ - f^-) - \frac{1}{\omega_{nfs}}\frac{M}{M_{nfs}}(M_{nfs} - s\kappa_f e_f B)\left(-\frac{\partial f^+}{\partial M} - \frac{\partial f^-}{\partial M}\right)\right], \tag{C12}$$

$$X_\phi = 6G\sum_{nfs}\frac{|e_f B|}{2\pi}\int_{-\infty}^{+\infty}\frac{dp_z}{2\pi}\frac{1}{\omega_{nfs}}\frac{M}{M_{nfs}}(M_{nfs} - s\kappa_f e_f B)\left(\frac{\partial f^+}{\partial \phi} + \frac{\partial f^-}{\partial \phi}\right), \tag{C13}$$

$$X_{\bar{\Phi}} = 6G\sum_{nfs}\frac{|e_f B|}{2\pi}\int_{-\infty}^{+\infty}\frac{dp_z}{2\pi}\frac{1}{\omega_{nfs}}\frac{M}{M_{nfs}}(M_{nfs} - s\kappa_f e_f B)\left(\frac{\partial f^+}{\partial \bar{\phi}} + \frac{\partial f^-}{\partial \bar{\phi}}\right), \tag{C14}$$

$$X_T = -6G\sum_{nfs}\frac{|e_f B|}{2\pi}\int_{-\infty}^{+\infty}\frac{dp_z}{2\pi}\frac{1}{\omega_{nfs}}\frac{M}{M_{nfs}}(M_{nfs} - s\kappa_f e_f B)\left(\frac{\partial f^+}{\partial T} + \frac{\partial f^-}{\partial T}\right), \tag{C15}$$

$$X_{\mu_q} = -6G\sum_{nfs}\frac{|e_f B|}{2\pi}\int_{-\infty}^{+\infty}\frac{dp_z}{2\pi}\frac{1}{\omega_{nfs}}\frac{M}{M_{nfs}}(M_{nfs} - s\kappa_f e_f B)\left(\frac{\partial f^+}{\partial \mu_q} + \frac{\partial f^-}{\partial \mu_q}\right), \tag{C16}$$

$$Y_M = -3T\sum_{nfs}\frac{|e_f B|}{2\pi}\int_{-\infty}^{+\infty}\frac{dp_z}{2\pi}\left[-\frac{e^{-\frac{\omega_{nfs}-\mu_q}{T}}}{(g^+)^2}\frac{\partial g^+}{\partial M} - \frac{e^{-\frac{\omega_{nfs}-\mu_q}{T}}}{Tg^+}\frac{\partial\omega_{nfs}}{\partial M} - \frac{e^{-2\frac{\omega_{nfs}+\mu_q}{T}}}{(g^-)^2}\frac{\partial g^-}{\partial M} - \frac{2e^{-2\frac{\omega_{nfs}+\mu_q}{T}}}{Tg^-}\frac{\partial\omega_{nfs}}{\partial M}\right], \tag{C17}$$

$$Y_\phi = \frac{\partial^2 U}{\partial\phi^2} - 3T\sum_{nfs}\frac{|e_f B|}{2\pi}\int_{-\infty}^{+\infty}\frac{dp_z}{2\pi}\left[-\frac{e^{-\frac{\omega_{nfs}-\mu_q}{T}}}{(g^+)^2}\frac{\partial g^+}{\partial\phi} - \frac{e^{-2\frac{\omega_{nfs}+\mu_q}{T}}}{(g^-)^2}\frac{\partial g^-}{\partial\phi}\right], \tag{C18}$$

$$Y_{\bar{\Phi}} = \frac{\partial^2 U}{\partial\Phi\partial\bar{\Phi}} - 3T\sum_{nfs}\frac{|e_f B|}{2\pi}\int_{-\infty}^{+\infty}\frac{dp_z}{2\pi}\left[-\frac{e^{-\frac{\omega_{nfs}-\mu_q}{T}}}{(g^+)^2}\frac{\partial g^+}{\partial\bar{\Phi}} - \frac{e^{-2\frac{\omega_{nfs}+\mu_q}{T}}}{(g^-)^2}\frac{\partial g^-}{\partial\bar{\Phi}}\right], \tag{C19}$$

$$Y_T = -\frac{\partial^2 U}{\partial T\partial\Phi} + \sum_{nfs}\frac{|e_f B|}{2\pi}\int_{-\infty}^{+\infty}\frac{dp_z}{2\pi}\left[3\left\{\frac{e^{-\frac{\omega_{nfs}-\mu}{T}}}{g^+} + \frac{e^{-2\frac{\omega_{nfs}+\mu}{T}}}{g^-}\right\}\right.$$
$$\left. + 3T\left\{\frac{\omega_{nfs}-\mu_q}{T^2}\frac{e^{-\frac{\omega_{nfs}-\mu_q}{T}}}{g^+} - \frac{e^{-\frac{\omega_{nfs}-\mu_q}{T}}}{(g^+)^2}\frac{\partial g^+}{\partial T} + 2\frac{\omega_{nfs}+\mu_q}{T^2}\frac{e^{-2\frac{\omega_{nfs}+\mu_q}{T}}}{g^-} - \frac{e^{-2\frac{\omega_{nfs}+\mu_q}{T}}}{(g^+)^2}\frac{\partial g^-}{\partial T}\right\}\right], \tag{C20}$$

$$Y_\mu = 3T\sum_{nfs}\frac{|e_f B|}{2\pi}\int_{-\infty}^{+\infty}\frac{dp_z}{2\pi}\left\{\frac{e^{-\frac{\omega_{nfs}-\mu_q}{T}}}{Tg^+} - \frac{e^{-\frac{\omega_{nfs}-\mu_q}{T}}}{(g^+)^2}\frac{\partial g^+}{\partial\mu_q} - \frac{2e^{-2\frac{\omega_{nfs}+\mu_q}{T}}}{Tg^-} - \frac{e^{-2\frac{\omega_{nfs}+\mu_q}{T}}}{(g^-)^2}\frac{\partial g^-}{\partial\mu_q}\right\}, \tag{C21}$$

$$Z_M = -3T\sum_{nfs}\frac{|e_fB|}{2\pi}\int_{-\infty}^{+\infty}\frac{dp_z}{2\pi}\left[-\frac{2e^{-2\frac{\omega_{nfs}-\mu_q}{T}}}{Tg^+}\frac{\partial\omega_{nfs}}{\partial M}-\frac{e^{-2\frac{\omega_{nfs}-\mu_q}{T}}}{(g^+)^2}\frac{\partial g^+}{\partial M}-\frac{e^{-\frac{\omega_{nfs}+\mu_q}{T}}}{Tg^-}\frac{\partial\omega_{nfs}}{\partial M}-\frac{e^{-\frac{\omega_{nfs}+\mu_q}{T}}}{(g^-)^2}\frac{\partial g^-}{\partial M}\right], \tag{C22}$$

$$Z_\Phi = \frac{\partial^2 U}{\partial\Phi\bar{\Phi}}-3T\sum_{nfs}\frac{|e_fB|}{2\pi}\int_{-\infty}^{+\infty}\frac{dp_z}{2\pi}\left[-\frac{e^{-2\frac{\omega_{nfs}-\mu_q}{T}}}{(g^+)^2}\frac{\partial g^+}{\partial\Phi}-\frac{e^{-\frac{\omega_{nfs}+\mu_q}{T}}}{(g^-)^2}\frac{\partial g^-}{\partial\Phi}\right], \tag{C23}$$

$$Z_{\bar{\Phi}} = \frac{\partial^2 U}{\partial\bar{\Phi}^2}-3T\sum_{nfs}\frac{|e_fB|}{2\pi}\int_{-\infty}^{+\infty}\frac{dp_z}{2\pi}\left[-\frac{e^{-2\frac{\omega_{nfs}-\mu_q}{T}}}{(g^+)^2}\frac{\partial g^+}{\partial\bar{\Phi}}-\frac{e^{-\frac{\omega_{nfs}+\mu_q}{T}}}{(g^-)^2}\frac{\partial g^-}{\partial\bar{\Phi}}\right], \tag{C24}$$

$$Z_T = -\frac{\partial^2 U}{\partial T\partial\bar{\Phi}}+\sum_{nfs}\frac{|e_fB|}{2\pi}\int_{-\infty}^{+\infty}\frac{dp_z}{2\pi}\left[3\left\{\frac{e^{-2\frac{\omega_{nfs}-\mu_q}{T}}}{g^+}+\frac{e^{-\frac{\omega_{nfs}+\mu_q}{T}}}{g^-}\right\}\right. \tag{C25}$$

$$\left.+3T\left\{-\frac{e^{-2\frac{\omega_{nfs}-\mu_q}{T}}}{(g^+)^2}\frac{\partial g^+}{\partial T}+\frac{2(\omega_{nfs}-\mu_q)}{T^2}\frac{e^{-2\frac{\omega_{nfs}-\mu_q}{T}}}{g^+}-\frac{e^{-\frac{\omega_{nfs}+\mu_q}{T}}}{(g^-)^2}\frac{\partial g^-}{\partial T}+\frac{\omega_{nfs}+\mu_q}{T^2}\frac{e^{-\frac{\omega_{nfs}+\mu_q}{T}}}{g^-}\right\}\right], \tag{C26}$$

$$Z_{\mu_q} = 3T\sum_{nfs}\frac{|e_fB|}{2\pi}\int_{-\infty}^{+\infty}\frac{dp_z}{2\pi}\left[\frac{2e^{-2\frac{\omega_{nfs}-\mu_q}{T}}}{Tg^+}-\frac{e^{-\frac{\omega_{nfs}+\mu_q}{T}}}{Tg^-}-\frac{e^{-2\frac{\omega_{nfs}-\mu_q}{T}}}{(g^+)^2}\frac{\partial g^+}{\partial\mu_q}-\frac{e^{-\frac{\omega_{nfs}+\mu_q}{T}}}{(g^-)^2}\frac{\partial g^-}{\partial\mu_q}\right]. \tag{C27}$$

[1] D. E. Kharzeev, L. D. McLerran, and H. J. Warringa, Nucl. Phys. **A803**, 227 (2008).
[2] V. Skokov, A. Y. Illarionov, and V. Toneev, Int. J. Mod. Phys. A **24**, 5925 (2009).
[3] K. Tuchin, Phys. Rev. C **88**, 024911 (2013).
[4] U. Gursoy, D. Kharzeev, and K. Rajagopal, Phys. Rev. C **89**, 054905 (2014).
[5] G. Inghirami, L. Del Zanna, A. Beraudo, M. H. Moghaddam, F. Becattini, and M. Bleicher, Eur. Phys. J. C **76**, 659 (2016).
[6] P. Kalikotay, S. Ghosh, N. Chaudhuri, P. Roy, and S. Sarkar, Phys. Rev. D **102**, 076007 (2020).
[7] Frank Wilczek, *The CBM Physics Book: Compressed Baryonic Matter in Laboratory Experiments*, edited by B. Friman, C. Hohne, J. Knoll, S. Leupold, J. Randrup, R. Rapp, and P. Senger (Springer-Verlag Berlin Heidelberg, 2011), Vol. 814.
[8] V. A. Miransky and I. A. Shovkovy, Phys. Rep. **576**, 1 (2015).
[9] D. E. Kharzeev and K. Landsteiner, *Strongly Interacting Matter in Magnetic Fields*, edited by D. Kharzeev, K. Landsteiner, A. Schmitt, and H.-U. Yee (Springer-Verlag Berlin Heidelberg, 2013), Vol. 871.
[10] S. Chatrchyan *et al.* (CMS Collaboration), J. High Energy Phys. 05 (2012) 055.
[11] K. Fukushima, D. E. Kharzeev, and H. J. Warringa, Phys. Rev. D **78**, 074033 (2008).
[12] D. E. Kharzeev and H. J. Warringa, Phys. Rev. D **80**, 034028 (2009).
[13] I. A. Shovkovy, Lect. Notes Phys. **871**, 13 (2013).
[14] V. P. Gusynin, V. A. Miransky, and I. A. Shovkovy, Phys. Rev. Lett. **73**, 3499 (1994); **76**, 1005(E) (1996).
[15] V. P. Gusynin, V. A. Miransky, and I. A. Shovkovy, Nucl. Phys. **B462**, 249 (1996).
[16] V. P. Gusynin, V. A. Miransky, and I. A. Shovkovy, Nucl. Phys. **B563**, 361 (1999).
[17] F. Preis, A. Rebhan, and A. Schmitt, J. High Energy Phys. 03 (2011) 033.
[18] F. Preis, A. Rebhan, and A. Schmitt, Lect. Notes Phys. **871**, 51 (2013).
[19] S. Muroya, A. Nakamura, C. Nonaka, and T. Takaishi, Prog. Theor. Phys. **110**, 615 (2003).
[20] Y. Aoki, Z. Fodor, S. D. Katz, and K. K. Szabo, Phys. Lett. B **643**, 46 (2006).
[21] A. Bazavov *et al.*, Phys. Rev. D **80**, 014504 (2009).
[22] M. Cheng *et al.*, Phys. Rev. D **77**, 014511 (2008).
[23] S. P. Klevansky, Rev. Mod. Phys. **64**, 649 (1992).
[24] U. Vogl and W. Weise, Prog. Part. Nucl. Phys. **27**, 195 (1991).
[25] M. Buballa, Phys. Rep. **407**, 205 (2005).
[26] Y. Nambu and G. Jona-Lasinio, Phys. Rev. **124**, 246 (1961).
[27] Y. Nambu and G. Jona-Lasinio, Phys. Rev. **122**, 345 (1961).
[28] J. Bijnens, Phys. Rep. **265**, 369 (1996).
[29] C. Ratti, M. A. Thaler, and W. Weise, Phys. Rev. D **73**, 014019 (2006).
[30] C. Ratti, S. Roessner, M. A. Thaler, and W. Weise, Eur. Phys. J. C **49**, 213 (2007).

[31] J. O. Andersen, W. R. Naylor, and A. Tranberg, Rev. Mod. Phys. **88**, 025001 (2016).
[32] N. Chaudhuri, S. Ghosh, S. Sarkar, and P. Roy, Eur. Phys. J. A **56**, 213 (2020).
[33] R. Gatto and M. Ruggieri, Phys. Rev. D **82**, 054027 (2010).
[34] K. Fukushima, Phys. Rev. D **77**, 114028 (2008); **78**, 039902(E) (2008).
[35] O. A. Mattos, T. Frederico, and O. Lourenço, Eur. Phys. J. C **81**, 24 (2021).
[36] O. A. Mattos, T. Frederico, C. H. Lenzi, M. Dutra, and O. Lourenço, Phys. Rev. D **104**, 116001 (2021).
[37] Y. Wang and X.-J. Wen, Phys. Rev. D **105**, 074034 (2022).
[38] G. S. Bali, F. Bruckmann, G. Endrodi, Z. Fodor, S. D. Katz, S. Krieg, A. Schafer, and K. K. Szabo, J. High Energy Phys. 02 (2012) 044.
[39] G. S. Bali, S. Collins, M. Deka, B. Glassle, M. Gockeler, J. Najjar, A. Nobile, D. Pleiter, A. Schafer, and A. Sternbeck, Phys. Rev. D **86**, 054504 (2012).
[40] A. Bandyopadhyay and R. L. S. Farias, Eur. Phys. J. Special Topics **230**, 719 (2021).
[41] M. Ferreira, P. Costa, O. Lourenço, T. Frederico, and C. Providência, Phys. Rev. D **89**, 116011 (2014).
[42] R. L. S. Farias, V. S. Timoteo, S. S. Avancini, M. B. Pinto, and G. Krein, Eur. Phys. J. A **53**, 101 (2017).
[43] S. S. Avancini, R. L. Farias, and W. R. Tavares, Phys. Rev. D **99**, 056009 (2019).
[44] B.-k. Sheng, X. Wang, and L. Yu, Phys. Rev. D **105**, 034003 (2022).
[45] S. Mao, Phys. Lett. B **758**, 195 (2016).
[46] S. Fayazbakhsh and N. Sadooghi, Phys. Rev. D **90**, 105030 (2014).
[47] N. Chaudhuri, S. Ghosh, S. Sarkar, and P. Roy, Phys. Rev. D **99**, 116025 (2019).
[48] N. Chaudhuri, S. Ghosh, S. Sarkar, and P. Roy, Phys. Rev. D **103**, 096021 (2021).
[49] N. Chaudhuri, A. Mukherjee, S. Ghosh, S. Sarkar, and P. Roy, Eur. Phys. J. A **58**, 82 (2022).
[50] S. Ghosh, N. Chaudhuri, S. Sarkar, and P. Roy, Phys. Rev. D **101**, 096002 (2020).
[51] K. Xu, J. Chao, and M. Huang, Phys. Rev. D **103**, 076015 (2021).
[52] J. Mei and S. Mao, Phys. Rev. D **102**, 114035 (2020).
[53] R. M. Aguirre, Eur. Phys. J. A **57**, 166 (2021).
[54] S. Ghosh, N. Chaudhuri, P. Roy, and S. Sarkar, Phys. Rev. D **103**, 116008 (2021).
[55] R. L. S. Farias, W. R. Tavares, R. M. Nunes, and S. S. Avancini, Eur. Phys. J. C **82**, 674 (2022).
[56] E. J. Ferrer, V. de la Incera, J. P. Keith, I. Portillo, and P. L. Springsteen, Phys. Rev. C **82**, 065802 (2010).
[57] E. J. Ferrer and A. Hackebill, Int. J. Mod. Phys. A **37**, 2250048 (2022).
[58] E. J. Ferrer and A. Hackebill, Nucl. Phys. **A1031**, 122608 (2023).
[59] N. Chaudhuri, S. Ghosh, P. Roy, and S. Sarkar, Phys. Rev. D **106**, 056020 (2022).
[60] D. Chatterjee, T. Elghozi, J. Novak, and M. Oertel, Mon. Not. R. Astron. Soc. **447**, 3785 (2015).
[61] V. Canuto and H. Y. Chiu, Phys. Rev. **173**, 1210 (1968).
[62] A. P. Martinez, H. P. Rojas, and H. J. Mosquera Cuesta, Eur. Phys. J. C **29**, 111 (2003).
[63] J. L. Noronha and I. A. Shovkovy, Phys. Rev. D **76**, 105030 (2007); **86**, 049901(E) (2012).
[64] X.-G. Huang, M. Huang, D. H. Rischke, and A. Sedrakian, Phys. Rev. D **81**, 045015 (2010).
[65] M. Strickland, V. Dexheimer, and D. P. Menezes, Phys. Rev. D **86**, 125032 (2012).
[66] V. Dexheimer, D. P. Menezes, and M. Strickland, J. Phys. G **41**, 015203 (2014).
[67] M. Sinha, X.-G. Huang, and A. Sedrakian, Phys. Rev. D **88**, 025008 (2013).
[68] D. Peres Menezes and L. Laércio Lopes, Eur. Phys. J. A **52**, 17 (2016).
[69] D. P. Menezes, M. B. Pinto, and C. Providência, Phys. Rev. C **91**, 065205 (2015).
[70] E. J. Ferrer, V. de la Incera, D. Manreza Paret, A. Pérez Martínez, and A. Sanchez, Phys. Rev. D **91**, 085041 (2015).
[71] A. Bazavov *et al.* (HotQCD Collaboration), Phys. Lett. B **795**, 15 (2019).
[72] S. Borsanyi, Z. Fodor, J. N. Guenther, R. Kara, S. D. Katz, P. Parotto, A. Pasztor, C. Ratti, and K. K. Szabo, Phys. Rev. Lett. **125**, 052001 (2020).
[73] O. Philipsen, Prog. Part. Nucl. Phys. **70**, 55 (2013).
[74] Y. Aoki, G. Endrodi, Z. Fodor, S. D. Katz, and K. K. Szabo, Nature (London) **443**, 675 (2006).
[75] A. Bazavov *et al.* (HotQCD Collaboration), Phys. Rev. D **90**, 094503 (2014).
[76] K. Goswami, D. Sahu, J. Dey, R. Sahoo, and R. Stock, Phys. Rev. D **109**, 074012 (2024).
[77] W.-b. He, G.-y. Shao, X.-y. Gao, X.-r. Yang, and C.-l. Xie, Phys. Rev. D **105**, 094024 (2022).
[78] R. Marty, E. Bratkovskaya, W. Cassing, J. Aichelin, and H. Berrehrah, Phys. Rev. C **88**, 045204 (2013).
[79] J. Peterson, P. Costa, R. Kumar, V. Dexheimer, R. Negreiros, and C. Providencia, Phys. Rev. D **108**, 063011 (2023).
[80] A. Abhishek, H. Mishra, and S. Ghosh, Phys. Rev. D **97**, 014005 (2018).
[81] B.-J. Schaefer, M. Wagner, and J. Wambach, Phys. Rev. D **81**, 074013 (2010).
[82] R. Venugopalan and M. Prakash, Nucl. Phys. **A546**, 718 (1992).
[83] M. Bluhm, P. Alba, W. Alberico, A. Beraudo, and C. Ratti, Nucl. Phys. **A929**, 157 (2014).
[84] Z. V. Khaidukov, M. S. Lukashov, and Y. A. Simonov, Phys. Rev. D **98**, 074031 (2018).
[85] Z. V. Khaidukov and Y. A. Simonov, Phys. Rev. D **100**, 076009 (2019).
[86] S. Pal and G. Chaudhuri, Phys. Rev. D **108**, 103028 (2023).
[87] S. Pal, S. Podder, D. Sen, and G. Chaudhuri, Phys. Rev. D **107**, 063019 (2023).
[88] V. Mykhaylova and C. Sasaki, Phys. Rev. D **103**, 014007 (2021).
[89] F. Özel and P. Freire, Annu. Rev. Astron. Astrophys. **54**, 401 (2016).
[90] P. Bedaque and A. W. Steiner, Phys. Rev. Lett. **114**, 031103 (2015).

[91] I. Tews, J. Carlson, S. Gandolfi, and S. Reddy, Astrophys. J. **860**, 149 (2018).
[92] L. McLerran and S. Reddy, Phys. Rev. Lett. **122**, 122701 (2019).
[93] Y. Fujimoto, K. Fukushima, and K. Murase, Phys. Rev. D **101**, 054016 (2020).
[94] P. Jaikumar, A. Semposki, M. Prakash, and C. Constantinou, Phys. Rev. D **103**, 123009 (2021).
[95] B. P. Dolan, Phys. Rev. D **84**, 127503 (2011).
[96] A. Bhattacharyya, S. K. Ghosh, S. Majumder, and R. Ray, Phys. Rev. D **86**, 096006 (2012).
[97] M. Iwasaki, Phys. Rev. D **70**, 114031 (2004).
[98] L. Yang and X.-J. Wen, Phys. Rev. D **104**, 114010 (2021).
[99] H.-T. Ding, S.-T. Li, J.-H. Liu, and X.-D. Wang, Acta Phys. Pol. B Proc. Suppl. **16**, 1 (2023).
[100] H.-T. Ding, J.-B. Gu, A. Kumar, S.-T. Li, and J.-H. Liu, Phys. Rev. Lett. **132**, 201903 (2024).
[101] M. Marczenko, M. Szymański, P. M. Lo, B. Karmakar, P. Huovinen, C. Sasaki, and K. Redlich, arXiv:2405.15745.
[102] V. Vovchenko, arXiv:2405.16306.
[103] R. Mondal, N. Chaudhuri, P. Roy, and S. Sarkar, Phys. Rev. C **109**, 054911 (2024).
[104] S. Roessner, C. Ratti, and W. Weise, Phys. Rev. D **75**, 034007 (2007).
[105] K. Fukushima, M. Ruggieri, and R. Gatto, Phys. Rev. D **81**, 114031 (2010).
[106] J. I. Kapusta and C. Gale, *Finite-Temperature Field Theory: Principles and Applications*, Cambridge Monographs on Mathematical Physics (Cambridge University Press, Cambridge, England, 2011).
[107] R. Gatto and M. Ruggieri, Phys. Rev. D **83**, 034016 (2011).
[108] C. Sasaki, B. Friman, and K. Redlich, Phys. Rev. D **75**, 074013 (2007).
[109] N. Yao, A. Sorensen, V. Dexheimer, and J. Noronha-Hostler, Phys. Rev. C **109**, 065803 (2024).
[110] A. Sorensen, D. Oliinychenko, V. Koch, and L. McLerran, Phys. Rev. Lett. **127**, 042303 (2021).
[111] C. M. Hung and E. V. Shuryak, Phys. Rev. Lett. **75**, 4003 (1995).